

**ENHANCED CONDUCTIVITY OF
BLOCK COPOLYMER ELECTROLYTES
FOR LITHIUM BATTERIES**

by

Ellen H. Reed

A thesis submitted to the Faculty of the University of Delaware in partial fulfillment of the requirements for the degree of Honors Bachelor of Chemical Engineering with Distinction

Spring 2014

© 2014 Ellen H. Reed
All Rights Reserved

**ENHANCED CONDUCTIVITY OF
BLOCK COPOLYMER ELECTROLYTES
FOR LITHIUM BATTERIES**

by

Ellen H. Reed

Approved: _____
Thomas H. Epps, III, Ph.D.
Professor in charge of thesis on behalf of the Advisory Committee

Approved: _____
Eric Furst, Ph.D.
Committee member from the Department of Chemical and Biomolecular
Engineering

Approved: _____
Norbert Mulders, Ph.D.
Committee member from the Board of Senior Thesis Readers

Approved: _____
Michael Arnold, Ph.D.
Director, University Honors Program

ACKNOWLEDGMENTS

First and foremost, I would like to thank my advisor Prof. Thomas H. Epps, III for his guidance and advice throughout my undergraduate career. I am grateful for the opportunity to work in his group as it has made me a better scientist and solidified my decision to pursue a PhD. I would also like to thank Prof. Eric Furst for serving the second reader and Prof. Norbert Mulders for serving as the third reader.

Next, I would like to thank Wei-Fan Kuan, my graduate student mentor, for all his help with my research. He taught me many of the characterization techniques used in this work. Furthermore, he was always there when I had questions or needed help. I would also like to thank him for many helpful conversations along the way.

I would also like to thank the rest of the Epps group, including Dr. Matthew Green, Dr. Jon Seppala, Jillian Emerson, Angela Holmberg, Dr. Elizabeth Kelley, Ming Luo, Sarah Mastroianni, Michael Mayeda, Melody Morris, Ryan Murphy, Kaleigh Reno, Cameron Shelton, Eddie Sangern, Kevin Hutter, and Matthew Hoffman for their helpful conversations and encouragement. I would also like to thank Roddel Remy for all his help with differential scanning calorimetry.

Finally, I would like to thank my friends and family for their love and support throughout my undergraduate career.

TABLE OF CONTENTS

| | |
|---|-----|
| LIST OF TABLES | vi |
| LIST OF FIGURES | vii |
| ABSTRACT | x |
| | |
| 1 INTRODUCTION AND BACKGROUND | 1 |
| 1.1 Lithium Batteries | 1 |
| 1.2 Polymer Electrolytes | 3 |
| 1.2.1 Homopolymer Electrolytes..... | 5 |
| 1.2.2 Block Copolymer Electrolytes | 5 |
| 1.3 Thesis Overview | 8 |
| | |
| 2 MATERIALS AND METHODS | 10 |
| 2.1 Materials Synthesis..... | 10 |
| 2.2 Characterization..... | 11 |
| 2.2.1 Small Angle X-ray Scattering | 11 |
| 2.2.2 Differential Scanning Calorimetry | 13 |
| 2.2.3 Alternating Current Impedance Spectroscopy..... | 15 |
| 2.2.4 Transmission Electron Microscopy..... | 19 |
| | |
| 3 RESULTS AND DISCUSSION..... | 20 |
| 3.1 Copolymer/Copolymer Blends | 20 |
| 3.1.1 Small Angle X-ray Scattering | 21 |
| 3.1.2 Differential Scanning Calorimetry | 26 |
| 3.1.3 Alternating Current Impedance Spectroscopy..... | 29 |
| 3.1.4 Conclusions | 34 |
| 3.2 Nanoparticle Additives | 35 |
| 3.2.1 Transmission Electron Microscopy..... | 36 |
| 3.2.2 Differential Scanning Calorimetry | 38 |
| 3.2.3 Alternating Current Impedance Spectroscopy..... | 42 |

| | | |
|-------|--|----|
| 3.2.4 | Conclusions | 47 |
| 4 | THESIS SUMMARY AND RECOMMENDATIONS FOR FUTURE WORK | 48 |
| 4.1 | Copolymer/Copolymer Blends | 48 |
| 4.2 | Nanoparticle Additives | 48 |
| 4.3 | Recommendations for Future Work | 49 |
| | REFERENCES | 50 |
| | COPYRIGHT PERMISSIONS | 52 |

LIST OF TABLES

| | | |
|------------|--|----|
| Table 2.1: | Relative peak ratios for various block copolymer morphologies..... | 13 |
| Table 3.1: | Molecular weight and composition of PS-PEO and PS-POEM..... | 20 |
| Table 3.2: | Composition of PS-PEO/PS-POEM copolymer/copolymer blends..... | 21 |
| Table 3.3: | Domain spacing for PS-PEO, PS-POEM, and copolymer/copolymer blends from SAXS data. Spacing is given for both neat and salt doped samples..... | 25 |
| Table 3.4: | Melting temperature, heat of fusion, and percent crystallinity for PS-PEO, PS-POEM, and copolymer/copolymer blends as found from DSC..... | 27 |
| Table 3.5: | Activation energy and pre-exponential for PS-PEO, PS-POEM, and copolymer/copolymer blends found from least squares fitting of conductivity data..... | 32 |
| Table 3.7: | Melting temperature, heat of fusion, and percent crystallinity for PS-PEO-PS, LiCF ₃ SO ₃ , TiO ₂ samples as found from DSC. For all samples [EO]:[Li ⁺]=24:1. Titania compositions are given as EO:TiO ₂ mass ratios..... | 39 |
| Table 3.8: | Activation energy and pre-exponential for PS-PEO-PS and titania doped samples found from least squares fitting of conductivity data..... | 45 |

LIST OF FIGURES

| | |
|--|----|
| Figure 1.1: Volumetric energy density versus gravimetric energy density for various commercially available batteries. Adapted from ref. 1. Copyright 2008 Nature Publishing Group..... | 1 |
| Figure 1.2: Schematic of lithium ion battery operation. Adapted from ref. 8. Copyright 2013 Wiley Periodicals, Inc. | 2 |
| Figure 1.3: Diagram of the movement of lithium ions through a polymer system. Adapted from ref. 6. Copyright 1998 WILEY-VCH Verlag GmbH, Weinheim, Fed. Rep. of Germany..... | 4 |
| Figure 1.4: Model phase diagram for diblock copolymer melts (top image) adapted from ref. 10. Copyright 2012 American Chemical Society. Morphologies for diblock copolymer melts (bottom image) adapted from ref. 11. Copyright 2012 The Royal Society of Chemistry..... | 6 |
| Figure 1.5: Chemical structure of polystyrene- <i>b</i> -poly(ethylene oxide) (top left image), polystyrene- <i>b</i> -poly(oligo(oxyethylene) methacrylate) (top right image), and polystyrene- <i>b</i> -poly(ethylene oxide)- <i>b</i> -polystyrene (bottom image). | 7 |
| Figure 2.1: Schematic of small angle X-ray scattering. Adapted from ref. 2. Copyright 2012 Wen-Shiue Young..... | 12 |
| Figure 2.2: Schematic of differential scanning calorimetry (DSC). Adapted from ref. 17. Copyright 2012 The University of Southern Mississippi. | 14 |
| Figure 2.3: Schematic of alternating current impedance spectroscopy sample cell. Adapted from ref. 2. Copyright 2012 Wen-Shiue Young. | 16 |
| Figure 2.4: Equivalent circuit for alternating current impedance spectroscopy sample cell showing geometric capacitance (C_g), double layer capacitance (C_{dl}), and bulk resistance of the electrolyte (R_b). Adapted from ref. 2. Copyright 2012 Wen-Shiue Young..... | 16 |
| Figure 2.5: Representative Nyquist (left) and Bode (right) plots. Adapted from ref. 2. Copyright 2012 Wen-Shiue Young. | 17 |

| | |
|--|----|
| Figure 3.1: SAXS profiles of PS-PEO and PS-POEM with and without LiCF ₃ SO ₃ . [EO]:[Li ⁺] = 24:1. Curves are shifted vertically for clarity..... | 22 |
| Figure 3.2: SAXS profiles of PS-PEO/PS-POEM copolymer/copolymer blends with and without LiCF ₃ SO ₃ . [EO]:[Li ⁺]=24:1. Curves are shifted vertically for clarity..... | 24 |
| Figure 3.3: DSC traces for PS-PEO, PS-POEM, and copolymer/copolymer blends. The 3 rd heating trace is shown with exothermic heat flow up. Samples were heated at a rate of 10 °C/min. Curves shifted vertically for clarity..... | 26 |
| Figure 3.4: Heat of fusion of PS-PEO and copolymer/copolymer blends as found from DSC plotted with respect to the weight fraction of PEO in the sample. Heat of fusion is normalized to the mass of PEO in the sample..... | 28 |
| Figure 3.5: Temperature dependent conductivity data for PS-PEO, PS-POEM, and copolymer/copolymer blends. Conductivity is plotted on a logarithmic scale with respect to inverse absolute temperature..... | 29 |
| Figure 3.6: Temperature dependent conductivity data for PS-PEO, PS-POEM, and copolymer/copolymer blends fitted to the VTF model. The activation energy was found from the slope and the pre-exponential was found from the y-intercept..... | 32 |
| Figure 3.7: Structure of oleic acid ligand bound to TiO ₂ nanoparticles..... | 36 |
| Figure 3.8: TEM images of oleic acid coated TiO ₂ nanoparticles..... | 36 |
| Figure 3.9: TEM images of TiO ₂ nanoparticles dispersed in the PS-PEO-PS matrix..... | 37 |
| Figure 3.10: DSC traces for PS-PEO-PS doped with LiCF ₃ SO ₃ and varying amounts of titania. For all samples [EO]:[Li ⁺]=24:1. Titania compositions are given as EO to TiO ₂ mass ratios. The 3 rd heating trace is shown with exothermic heat flow up. Samples were heated at a rate of 10 °C/min. Curves shifted vertically for clarity..... | 38 |
| Figure 3.11: Zoom in around 115 °C of DSC traces for PS-PEO-PS doped with LiCF ₃ SO ₃ and varying amounts of titania. Curves shifted vertically for clarity..... | 40 |

| | |
|---|----|
| Figure 3.12: PEO, LiCF ₃ SO ₃ phase diagram adapted from ref. 5. Copyright 2003 The Electrochemical Society. Arrow represents salt composition used in this work..... | 41 |
| Figure 3.13: Temperature dependent conductivity data for PS-PEO-PS doped with LiCF ₃ SO ₃ and varying amounts of titania. Conductivity is plotted on a logarithmic scale with respect to inverse absolute temperature. | 42 |
| Figure 3.14: Temperature dependent conductivity data for PS-PEO-PS and titania doped samples fitted to the VTF model. The activation energy was found from the slope and the pre-exponential was found from the y-intercept. | 44 |
| Figure 3.15: Temperature dependent conductivity data for PS-POEM doped with LiCF ₃ SO ₃ with and without titania. Conductivity is plotted on a logarithmic scale with respect to inverse absolute temperature. | 46 |
| Figure A.1: Copyright permission for Figure 1.1, battery energy densities. | 52 |
| Figure A.2: Copyright permission for Figure 1.2, lithium ion battery operation. | 53 |
| Figure A.3: Copyright permission for Figure 1.3, Movement of lithium ions through polymer system. | 54 |
| Figure A.4: Copyright permission for Figure 1.4, block copolymer phase diagram. . | 55 |
| Figure A.5: Copyright permission for Figure 1.4, block copolymer morphologies. .. | 56 |
| Figure A.5: Copyright permission for Figure 3.12, PEO:LiCF ₃ SO ₃ phase diagram. . | 57 |

ABSTRACT

Polymers are promising materials for ion conducting membranes in lithium and lithium ion batteries due to their mechanical strength and thermal and electrochemical stability. Poly(ethylene oxide) (PEO) based polymer electrolytes are candidates for this application; however, they show a discontinuity in conductivity around 60 °C due to crystallization. Below this temperature, the conductivity is markedly lower reducing the performance at room temperature. In this work, we explored two strategies for increasing the room temperature conductivity of PEO based electrolytes by inhibiting crystallization. The first approach was forming copolymer/copolymer blends with polystyrene-*b*-poly(ethylene oxide) (PS-PEO) and polystyrene-*b*-poly(oligo(oxyethylene) methacrylate) (PS-POEM). We found that the PS-POEM did not inhibit crystallization of PEO. However, due to its amorphous nature, PS-POEM was three orders of magnitude more conductive than PS-PEO. The second approach was adding titania nanoparticles to polystyrene-*b*-poly(ethylene oxide)-*b*-polystyrene (PS-PEO-PS). We found that the addition of titania nanoparticles reduced the crystallinity of the PEO block by 10% regardless of the titania to ethylene oxide ratio. Additionally, the room temperature conductivity increased upon nanoparticles addition. This increase was dependent upon composition, with highest increase noted for a doping ratio of 10:1 followed by 5:1 then 20:1.

Chapter 1

INTRODUCTION AND BACKGROUND

1.1 Lithium Batteries

Many types of batteries are currently commercially available, including lead-acid, nickel-cadmium, nickel-metal hydride, and lithium. Currently, lithium batteries are preferred due to their high gravimetric and volumetric energy density as compared to other systems as shown in Figure 1.1.¹

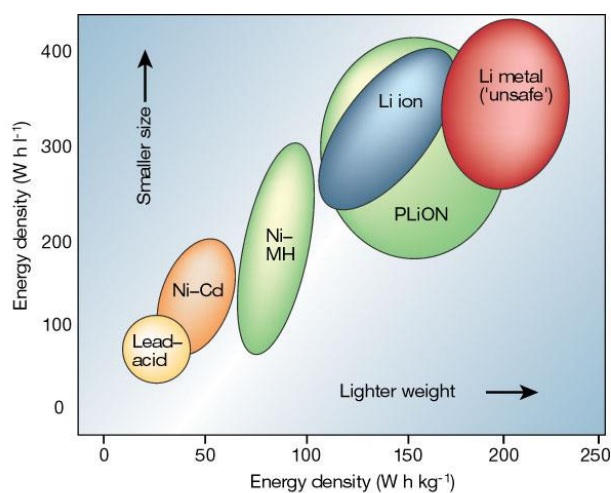


Figure 1.1: Volumetric energy density versus gravimetric energy density for various commercially available batteries. Adapted from ref. 1. Copyright 2008 Nature Publishing Group.

Both primary and secondary lithium batteries are widely utilized commercially. Primary (non-rechargeable) lithium batteries are employed in consumer products such as watches, calculators, cameras, and artificial pacemakers. Secondary (rechargeable) lithium batteries, also referred to as lithium ion batteries, are most notably applied in consumer electronics. Mobile phones, laptops, and electric vehicles all use lithium ion batteries.

The operation of a lithium ion battery is illustrated in Figure 1.2. Two electrodes, a negatively charged anode and a positively charged cathode, are separated by a conductive electrolyte. The two electrodes have different chemical potentials, which causes electrons to flow. During discharge, lithium is oxidized at the anode to create positively charged lithium cations. These cations migrate through the electrolyte and are reduced to lithium at the cathode. The electrons liberated from the lithium in this process can be used to do work before recombining with lithium ions at the cathode. During charging, an applied voltage causes this process to operate in reverse: lithium ions migrate from the cathode to the anode.^{1,2}

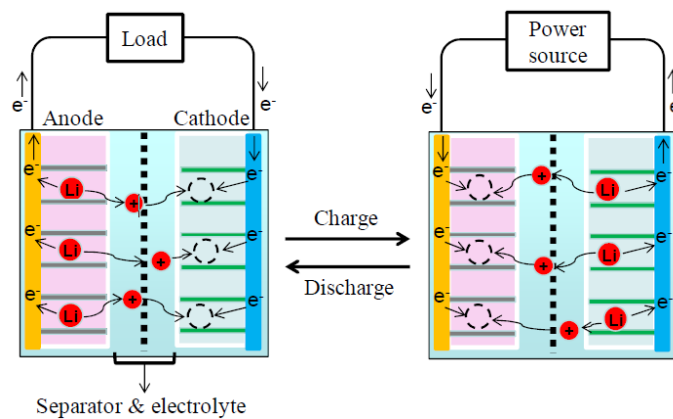


Figure 1.2: Schematic of lithium ion battery operation. Adapted from ref. 8. Copyright 2013 Wiley Periodicals, Inc.

Classically, the electrolytes for lithium and lithium ion batteries have been organic solvents such as propylene carbonate. The conductivity of these electrolytes is generally between 10^{-3} S/cm and 10^{-2} S/cm. However, liquid electrolytes pose safety concerns. Organic liquids are flammable and may ignite if the battery is heated or damaged. Liquid electrolytes may also leak from the cell. Furthermore during charge-discharge cycles, lithium dendrites may begin to grow on the electrodes potentially causing the battery to short circuit internally.³

There is a need for an electrolyte which has sufficient ionic conductivity, is thermally and electrochemically stable, has sufficient mechanical integrity, and inhibits dendrite formation. Efforts have been made to achieve this by reducing the amount of liquid in the electrolyte system and creating gel electrolytes. However, these systems also pose safety concerns as they may still lead to fire. Polymer electrolytes are gaining interest because they are non-volatile, are electrochemically stable, and have sufficient mechanical integrity to prevent dendrite formation.⁴

1.2 Polymer Electrolytes

A polymer is defined as a macromolecule composed of multiple chemically identical repeat units. Several polymers have been found to be conductive to lithium ions. The mechanism for ion conduction is shown schematically in Figure 1.3. Lithium ions form complexes with lone pairs on the ether oxygens. In the case of LiCF_3SO_3 and polyethylene oxide (PEO), three ethylene oxide groups form a complex with a lithium ion.⁵ The formation of complexes promotes the dissociation of the lithium cation from its anion. Lithium ions then move between complex sites as a result of segmental motion of the polymer chain.⁶

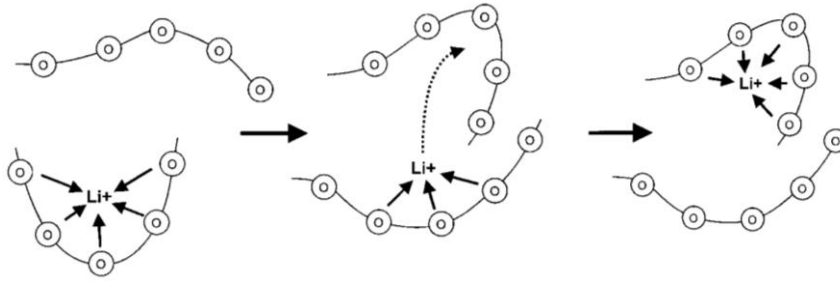


Figure 1.3: Diagram of the movement of lithium ions through a polymer system. Adapted from ref. 6. Copyright 1998 WILEY-VCH Verlag GmbH, Weinheim, Fed. Rep. of Germany.

The segmental motion of polymer chains, and therefore the conductivity, is dependent on temperature. This dependence can be modeled using the Vogel-Tammann-Fulcher (VTF) model given in Equation 1.1:

$$\sigma = AT^{-1/2} \exp \left\{ \frac{-B}{R(T-T_0)} \right\}, \quad 1.1$$

in which σ is conductivity, A is the pre-exponential factor (proportional to the number of charge carriers), T is absolute temperature, B is the apparent activation energy, R is the gas constant, and T_0 is the glass transition temperature of the ion solvating block of the polymer. The activation energy represents the energy required for a lithium ion to move between complex sites. The VTF model can be contrasted to a simple Arrhenius type model given in Equation 1.2:

$$\sigma = \sigma_0 \exp \left(\frac{-E_a}{RT} \right), \quad 1.2$$

in which σ_0 is the pre-exponential factor, and E_a is the activation energy. The dependence of $\log \sigma$ on T^{-1} in both models is attributed to the hopping motion of the lithium ions, whereas the nonlinear $T^{-1/2}$ term in the VTF model accounts for the segmental motion of the polymer chain. Therefore, the VTF model is most applicable

for amorphous polymers, and the Arrhenius relationship is most applicable for crystalline polymers.⁷

1.2.1 Homopolymer Electrolytes

Several ion conducting homopolymers have been identified such as polyethylene oxide (PEO) and polypropylene oxide (PPO). PEO has been widely studied due to its superior solvation of lithium salts. The conductivity of PEO has been shown to increase at lower molecular weights due to increased segmental motion of the polymer chains; however, lower molecular weights result in a decrease the mechanical strength. Thus, block copolymers with a rigid block have been used to overcome this barrier.⁸

1.2.2 Block Copolymer Electrolytes

A block copolymer consists of multiple homopolymers covalently linked together. The most notable property of block copolymers is the ability to phase separate on a nanometer scale. The resulting morphology of the polymer is dependent upon the degree of polymerization (N), the Flory-Huggins interaction parameter (χ), and the composition (f) as shown in Figure 1.4. The product of degree of polymerization and Flory-Huggins interaction parameter (χN) is referred to as the segregation strength. As the segregation strength is increased, the system moves from a disordered state to a phase separated, ordered state. Below the order-disorder transition temperature, the system is homogenous; above the order-disorder transition temperature, morphologies include spheres, cylinders, gyroid, and lamellae shown in Figure 1.4. Bulk morphology is dependent on the composition of the block copolymer.⁹⁻¹⁰⁻¹¹ Similar phenomena are noted for triblock copolymers.¹²

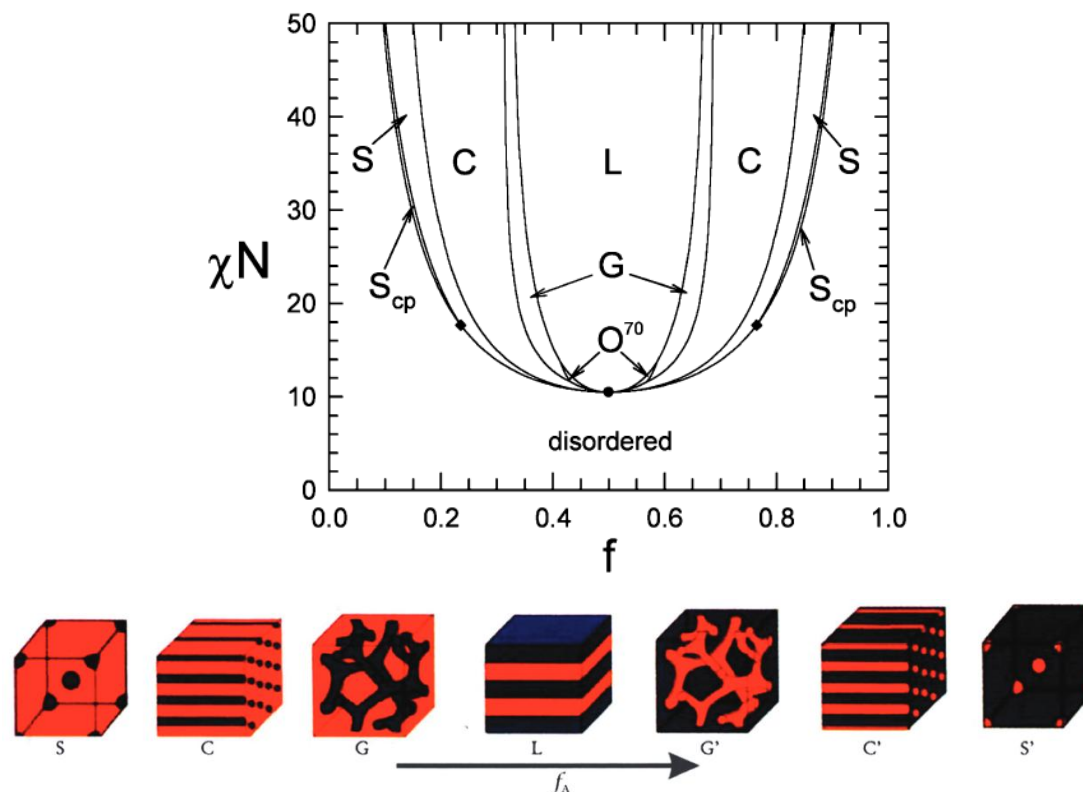


Figure 1.4: Model phase diagram for diblock copolymer melts (top image) adapted from ref. 10. Copyright 2012 American Chemical Society. Morphologies for diblock copolymer melts (bottom image) adapted from ref. 11. Copyright 2012 The Royal Society of Chemistry.

Block copolymer electrolytes consist of a conductive, ion solvating, block and a “hard” block. The hard block is rigid at the use temperature; therefore, it provides mechanical strength that is absent in homopolymer electrolytes. The conductivity of block copolymer electrolytes is dependent upon the morphology, because conductive pathways are formed by the ion solvating block of the electrolyte. These pathways are discontinuous because the electrolyte is composed of multiple grains. As a result, ion transport occurs both within grains and across grains. The movement of ions across grains is energetically unfavorable and causes a decrease in the conductivity. As a

result, ionic conductivity has been found to be higher for cylindrical morphologies than for lamellar morphologies, and higher still for gyroid morphologies as they have continuous conductive pathways.¹³

In this work, the ion solvating block was either poly(ethylene oxide) (PEO) or poly(oligo(oxyethylene) methacrylate) (POEM), and the hard block was polystyrene (PS). The chemical structures of the block copolymers used are shown in Figure 1.5.

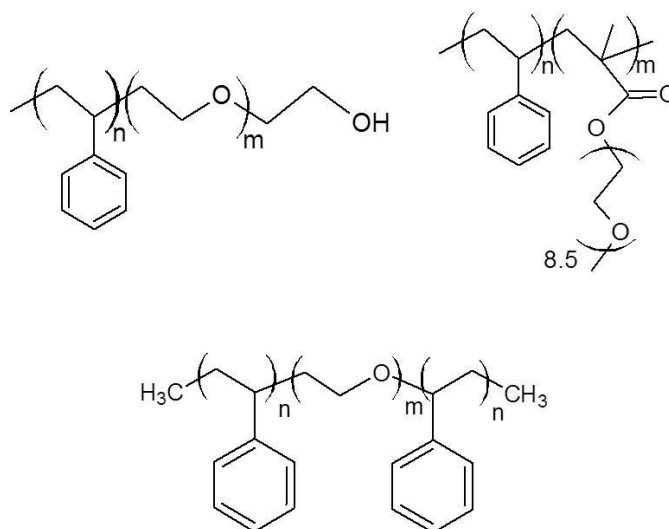


Figure 1.5: Chemical structure of polystyrene-*b*-poly(ethylene oxide) (top left image), polystyrene-*b*-poly(oligo(oxyethylene) methacrylate) (top right image), and polystyrene-*b*-poly(ethylene oxide)-*b*-polystyrene (bottom image).

Ultimately, conductivity is determined by the number of mobile ions in the system, the electric charge, and the ion mobility. Ion mobility is higher when there is more segmental motion of the polymer chains. Therefore, conduction is enhanced when the polymer chains are more mobile, i.e. in the amorphous phase. PEO crystallizes around 60 °C, resulting in significantly reduced conductivity below this temperature. However, to be commercially viable, polymer electrolytes need to be highly conductive at room temperature.

1.3 Thesis Overview

The goal of this work was to increase the room temperature conductivity of PEO based block copolymer electrolytes. Two strategies have been employed to increase the conductivity. Both of these strategies focus upon decreasing the degree of crystallinity of the PEO block. Decreasing the degree of crystallinity results in a higher percentage of amorphous material, and, consequently, higher conductivity. First, PS-PEO was blended with PS-POEM. Second, PS-PEO-PS was blended with titania nanoparticles.

PS-POEM is amorphous at room temperature due to the comb-like nature of the ethylene oxide side chains. These side chains are thought to inhibit crystallization. However, the short ethylene oxide side chains on the POEM have a lower amount of segmental motion than PEO.¹⁴ The block copolymers PS-PEO and PS-POEM were blended in various ratios with the goal of inhibiting the crystallization of the PEO while maintaining the conductivity.

The addition of nanoparticles is believed to reduce the degree of crystallinity as a result of the dispersed particles preventing organization of the polymer chains. The interactions between the particles and the polymer chain affect the kinetics for

reorganization and create amorphous regions.¹⁵ The triblock copolymer PS-PEO-PS was blended with titania nanoparticles in various ratios with the goal of increasing conductivity by increasing the size of the amorphous regions.

Chapter 2

MATERIALS AND METHODS

2.1 Materials Synthesis

The synthesis of the polymers used in this work was performed by Dr. Wen-Shiue Young, Dr. Raghunath Roy, or Wei-Fan Kuan using sequential anionic polymerization. First, the PS block was synthesized and capped with a hydroxyl group. Then, PS-OH was reinitiated to polymerize either ethylene oxide or ethylene glycol methyl ether methacrylate to yield PS-PEO or PS-POEM, respectively.² The resultant polymers were dried using a freeze-dry process and stored in the glovebox. The composition and molecular weight distribution were confirmed using gel permeation chromatography (GPC) and proton nuclear magnetic resonance (¹H NMR) spectroscopy.

Polymer blends were prepared in an argon filled glovebox to limit water absorption into the sample. Measured amounts of each polymer were combined and dissolved in tetrahydrofuran (THF). First, THF was first degassed using argon sparging and passed through two alumina columns. 1 mL of solvent was used per every 10 mg of polymer to ensure sufficient blending. Then, the vial containing this mixture was then placed in a drying chamber and removed from the glovebox. The mixture was dried under dynamic vacuum while stirring. After the sample was completely dry, it was stored in the glovebox.

The lithium salt used in this work was lithium trifluoromethanesulfonate (LiCF₃SO₃) which was obtained from Sigma-Aldrich, dried further under dynamic

vacuum, and stored in an argon filled glovebox. The salt-doped polymer samples were prepared in the glovebox. Measured amounts of LiCF_3SO_3 and polymer (or polymer blend) were each dissolved in THF and then combined. The vial containing this mixture was placed in a drying chamber and removed from the glovebox. The mixture was dried under dynamic vacuum while stirring. After the sample was completely dry, it was stored in the glovebox.

Anatase titania particles (TiO_2) coated with an oleic acid ligand courtesy of the Hammond group at the Massachusetts Institute of Technology were used in this work. Measured amounts of TiO_2 and polymer were combined and dissolved in THF. The vial containing this mixture was placed in a drying chamber and removed from the glovebox. The mixture was dried under dynamic vacuum while stirring. After the sample was completely dry, it was stored in the glovebox.

2.2 Characterization

2.2.1 Small Angle X-ray Scattering

Small angle X-ray scattering (SAXS) was used in this work to characterize the morphology of block copolymers and block copolymer blends. SAXS probes features in the 5 nm to 100 nm size scale. The setup of SAXS is shown schematically in Figure 2.1.

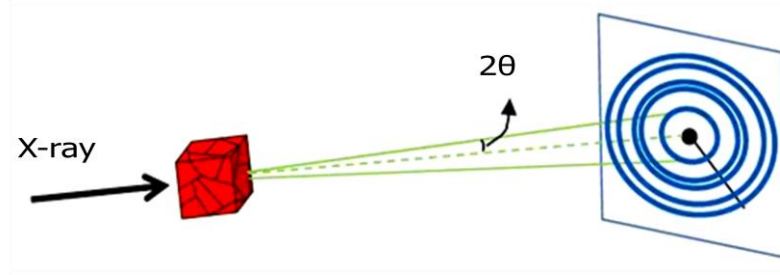


Figure 2.1: Schematic of small angle X-ray scattering. Adapted from ref. 2. Copyright 2012 Wen-Shiue Young.

A focused X-ray was passed through the sample, and the resultant scattering was recorded. Then, the 2-D scattering data were integrated azimuthally to obtain a 1-D plot of intensity vs. scattering wavevector. Wavevector is defined in Equation 2.1:

$$q = |q| = \frac{4\pi}{\lambda} \sin(\theta) , \quad 2.1$$

in which q is the scattering wavevector, λ is the X-ray wavelength, and θ is the Bragg reflection angle—half the angle between the incident and diffracted beam as shown in Figure 2.1.

The relationship between the polymer nanostructure and X-ray scattering is governed by Bragg's law given in Equation 2.2:

$$n\lambda = 2d \sin(\theta) , \quad 2.2$$

in which n is the order of diffraction, and d is the interplanar spacing, i.e. the distance between neighboring reflection planes. Combining Equations 2.1 and 2.2, the wavevector is related to the domain spacing as shown in Equation 2.3:

$$q/2\pi = n/d . \quad 2.3$$

Because the relative location of reflection planes is dependent on morphology, morphology can be determined from the relative position of the peaks in the 1-D plot. The peak ratios for various morphologies are given in Table 2.1.¹⁶

Table 2.1: Relative peak ratios for various block copolymer morphologies.

| Morphology | Peak Ratios (q/q^*) |
|-------------------|---|
| Lamellae | 1, 2, 3, 4, ... |
| Gyroid | $\sqrt{6}$, $\sqrt{8}$, $\sqrt{14}$, $\sqrt{16}$, ... |
| Cylinders | 1, $\sqrt{3}$, $\sqrt{4}$, $\sqrt{7}$, ... |
| Spheres | 1, $\sqrt{2}$, $\sqrt{3}$, $\sqrt{4}$, ... |

The domain spacing of can be determined from the location of the primary peak by rearrangement of Equation 2.3 for n equal to one given in Equation 2.4:

$$d = 2\pi/q^*, \quad 2.4$$

in which q^* is the primary peak. In this work, the SAXS instrument had a 2 kW Cu $K\alpha$ X-ray source with a wavelength of 1.514 Å, a three-pinhole collimation alignment system, and a 2 m sample-to-detector distance. Samples were prepared in an argon filled glovebox to limit water absorption into the sample and sealed in a stainless steel cell between Kapton films.

2.2.2 Differential Scanning Calorimetry

Differential scanning calorimetry (DSC) was used in this work to characterize the thermal properties of block copolymers and block copolymer blends. The setup of DSC is shown schematically in Figure 2.2.¹⁷

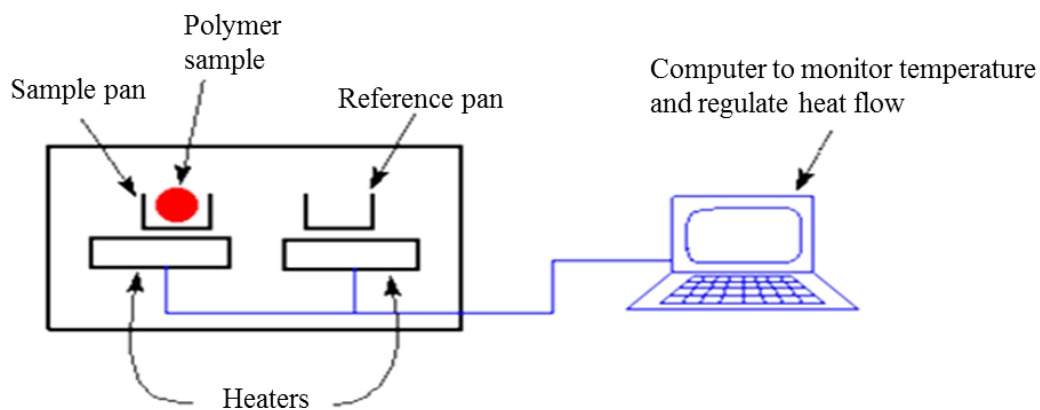


Figure 2.2: Schematic of differential scanning calorimetry (DSC). Adapted from ref. 17. Copyright 2012 The University of Southern Mississippi.

The sample and an empty reference pan both were heated at a constant rate by separate heaters. A computer monitored the power required by each heater to maintain a constant heating rate. The energy required to heat the sample pan and the reference pan were subtracted from one another to produce a plot of energy vs. temperature. Phase changes, such as melting and crystallization, as well as changes in heat capacity, e.g. glass transitions, appear as changes in energy required to heat the sample. An increase in the energy required is noted for endothermic phase changes, and a decrease in energy is noted for exothermic phase changes. Therefore, the temperature at which these changes occur can be determined.

Enthalpies of transition also can be determined from DSC. Enthalpies are found from integration under the curve corresponding to the phase transition. In this work, the heat of fusion was found from the area under the curve corresponding to melting as shown in Equation 2.5:

$$\Delta H_{fus} = \frac{A}{x} / \frac{\Delta T}{t}, \quad 2.5$$

in which ΔH_{fus} is the heat of fusion, A is the area under the curve, x is the weight fraction of material undergoing the phase transition, and $\Delta T/t$ is the rate of heating. The degree of crystallinity can be determined from the heat of fusion as shown in Equation 2.6:

$$X_c = \frac{\Delta H_{fus}}{\Delta H_{fus,p}}, \quad 2.6$$

in which X_c is the degree of crystallinity and $\Delta H_{fus,p}$ is the heat of fusion for the purely crystalline material—196 J/g for PEO.¹⁸

In this work, a TA Instruments Discovery DSC was used. Samples were prepared in an argon filled glovebox to limit water absorption into the sample. DSC traces were taken from -85 °C to 200 °C at a rate of 10 °C/min. Three heating and three cooling traces were taken for each sample. If water was present in the sample it could be seen in the first trace. The second and third traces were nearly identical; the third trace data are shown in this work.

2.2.3 Alternating Current Impedance Spectroscopy

Alternating current impedance (AC impedance) spectroscopy was used in this work to measure ionic conductivity. The setup of AC impedance spectroscopy is shown schematically in Figure 2.3.

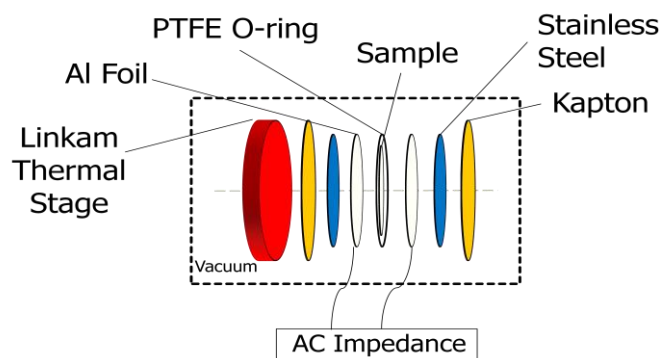


Figure 2.3: Schematic of alternating current impedance spectroscopy sample cell. Adapted from ref. 2. Copyright 2012 Wen-Shiue Young.

Impedance is the resistance to an alternating current by an electric circuit. Capacitors and resistors both contribute to impedance. This sample cell set-up results in geometric capacitance, double layer capacitance, and bulk resistance. The geometric capacitance is the result of the charges on the electrodes, the double layer capacitance is the result of the accumulation of charged ions in the electrolyte at the electrode-electrolyte interface, and the bulk resistance is a result of the electrolyte itself. The equivalent circuit is shown in Figure 2.4.

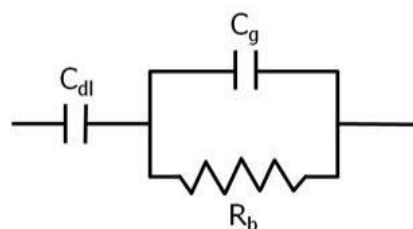


Figure 2.4: Equivalent circuit for alternating current impedance spectroscopy sample cell showing geometric capacitance (C_g), double layer capacitance (C_{dl}), and bulk resistance of the electrolyte (R_b). Adapted from ref. 2. Copyright 2012 Wen-Shiue Young.

The impedance from the electrolyte is equal to the bulk resistance, and the impedance of the capacitors is given in Equation 2.7:

$$Z_c = -j \frac{1}{2\pi f C}, \quad 2.7$$

in which Z is impedance, j is the unit imaginary number, f is the frequency of the AC current, and C is the capacitance. Combining the bulk resistance and the capacitance: the total impedance of the circuit shown in Figure 2.4, broken into real and imaginary parts, is given by Equation 2.8:

$$Z = \frac{R_b}{1+(2\pi f C_g R_b)^2} - j \frac{\left[1+(2\pi f C_g R_b)^2\right] \left(1+\frac{C_{dl}}{C_g}\right)}{2\pi f C_{dl} \left[1+(2\pi f C_g R_b)^2\right]}, \quad 2.8$$

in which R_b is the bulk resistance, C_g is the geometric capacitance, and C_{dl} is the double layer capacitance.

Impedance was found experimentally by applying an AC current to the cell at various frequencies and measuring the response. The real and imaginary parts of the impedance are represented graphically by Nyquist and Bode plots as shown in Figure 2.5.

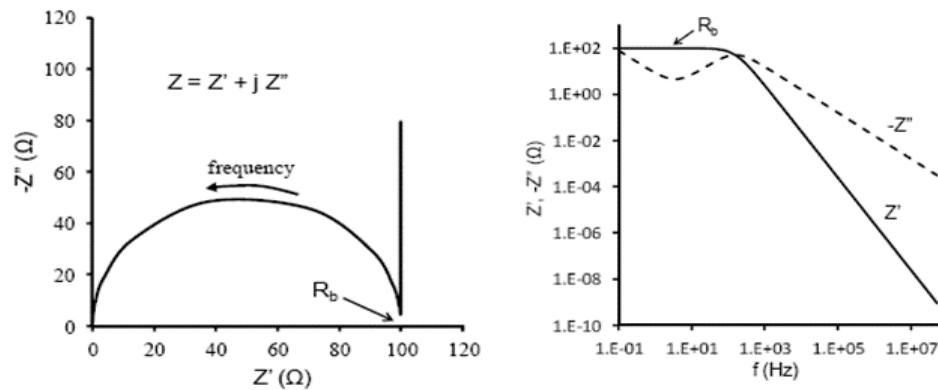


Figure 2.5: Representative Nyquist (left) and Bode (right) plots. Adapted from ref. 2. Copyright 2012 Wen-Shiue Young.

The bulk resistance is given by the touchdown point on the Nyquist plot and by the high frequency plateau on the Bode plot. As the conductivity increases, the touchdown point on the Nyquist plot and the plateau on the Bode plot appear at higher frequency positions. The conductivity is determined from bulk resistance as shown in Equation 2.9:

$$\sigma = L/R_b A , \quad 2.9$$

in which σ is conductivity, L is the sample thickness, and A is the contact area.

In this work, a Princeton Applied Research PARSTAT 2273 frequency response analyzer was used. Samples were prepared in an argon filled glovebox to limit water absorption into the sample. Samples were hot pressed under vacuum in the antechamber of the glovebox to create a disc. This disc was placed between aluminum foil electrodes using a Teflon O-ring as a spacer to create a sample cell. The sample thickness was taken to be the thickness of the O-ring spacer, 0.5 mm, and the surface area of the sample was taken to be the inside area of the O-ring, 0.32 cm². The test cell was placed in a Linkam HFS91 CAP stage and connected to temperature controllers. Measurements were taken using an AC frequency range of 0.1 to 1 MHz and a voltage of 10 mV upon heating at temperatures between 20 °C and 150 °C. Two measurements were taken at each temperature to ensure consistency. The second measurement was compared against the first to ensure that there was no change in conductivity due to temperature shift during the measurement. The first value is shown in this work.

2.2.4 Transmission Electron Microscopy

Transmission electron microscopy (TEM) was used in this work to confirm the morphology of block copolymers as determined by SAXS as well as to visualize the location of titania nanoparticles in the polymer. To create an image, electrons are generated using an electron gun and focused on a sample. These electrons are expanded onto the camera system after interacting with the sample. Electron density differences in the sample provide contrast. RuO₄ staining was used to enhance contrast. RuO₄ stains PEO more readily than PS affording greater contrast between the two blocks.

Chapter 3

RESULTS AND DISCUSSION

3.1 Copolymer/Copolymer Blends

The first method employed in this thesis work to enhance the conductivity of PS-PEO was forming copolymer/copolymer blends with PS-POEM. The molecular weight and composition of each polymer used are given in Table 3.1.

Table 3.1: Molecular weight and composition of PS-PEO and PS-POEM.

| polymer | $M_{n,PS}$ (g/mol) | wt. % PS |
|----------------|--------------------------------------|-----------------|
| PS-PEO | 22,400 | 56 |
| PS-POEM | 27,100 | 55 |

PS-POEM is a comb-like block copolymer and amorphous at room temperature; the short PEO side chains prevent the polymer chains from packing into crystals. However, the short side chains have a lower amount of segmental motion than linear PEO which is believed to lead to a decrease in the ionic conductivity.¹⁹ Copolymer/copolymer blends were made using PS-POEM and PS-PEO with the goal of enhancing conductivity by retaining the high conductivity of linear PEO while decreasing the crystallinity with POEM. Three copolymer/copolymer blends were made with compositions given in Table 3.2.

Table 3.2: Composition of PS-PEO/PS-POEM copolymer/copolymer blends.

| Sample | wt.% PS-POEM | wt.% PS-PEO |
|---------------|---------------------|--------------------|
| Blend I | 20 | 80 |
| Blend II | 50 | 50 |
| Blend III | 80 | 20 |

3.1.1 Small Angle X-ray Scattering

SAXS data for PS-PEO and PS-POEM with and without LiCF_3SO_3 are shown in Figure 3.1. Both salt doped samples had a 24:1 $[\text{EO}]:[\text{Li}^+]$ molar ratio. All four samples exhibited lamellar morphology as indicated by the peak locations. A lamellar morphology was expected as both block copolymers had nearly symmetric compositions.

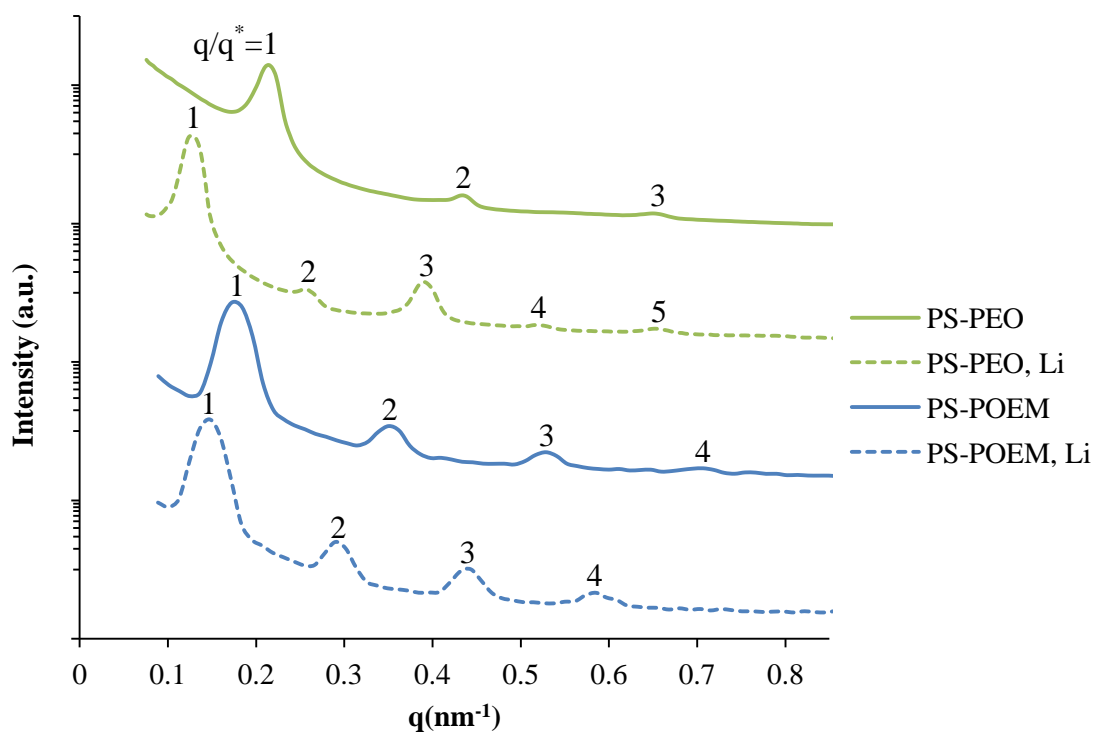


Figure 3.1: SAXS profiles of PS-PEO and PS-POEM with and without LiCF_3SO_3 . $[\text{EO}]:[\text{Li}^+] = 24:1$. Curves are shifted vertically for clarity.

The domain spacing for each sample as found from the location of the primary peak is given in Table 3.3. The domain spacing for PS-PEO was significantly smaller than that for PS-POEM: 29.3 nm and 37.7 nm, respectively. The larger domain spacing can be partially attributed to the larger molecular weight of the POEM block than the PEO block, 22,200 g/mol and 17,600 g/mol, respectively. The expected change in domain spacing for this increase is 17%, whereas a 29% increase was seen. The additional increase in domain spacing for PS-POEM can be attributed to the free volume associated with the short side chains on the POEM block.

For both PS-PEO and PS-POEM, the domain spacing increased upon salt doping. This increase can be attributed to both an increase in volume from the salt itself as well as chain stretching induced by the salt. The increase in volume from salt addition is minor, less than 10%; therefore, chain stretching accounts for most of the increase in domain spacing. The formation of lithium ion/ethylene oxide complexes stiffens the backbone of the polymer increasing the chain length.²⁰ The increase in domain spacing upon salt doping was larger for PS-PEO than for PS-POEM: 63% and 20% respectively. This result is likely due to the differing polymer structures. Ion complexation occurs on the backbone of PEO; whereas, it occurs on the side chains of POEM. As a result, chain stretching had a smaller contribution to the domain spacing in POEM than in PEO.

SAXS data for PS-PEO/PS-POEM blends with and without LiCF_3SO_3 are shown in Figure 3.2. All salt doped samples had a 24:1 [EO]:[Li⁺] molar ratio. All six samples exhibited a lamellar morphology as indicated by the peak locations. Lamellar structures were expected because both block copolymers in the blends had nearly symmetric compositions. Blend III showed a slight shoulder on the primary peak indicating that the morphology may be disrupted.

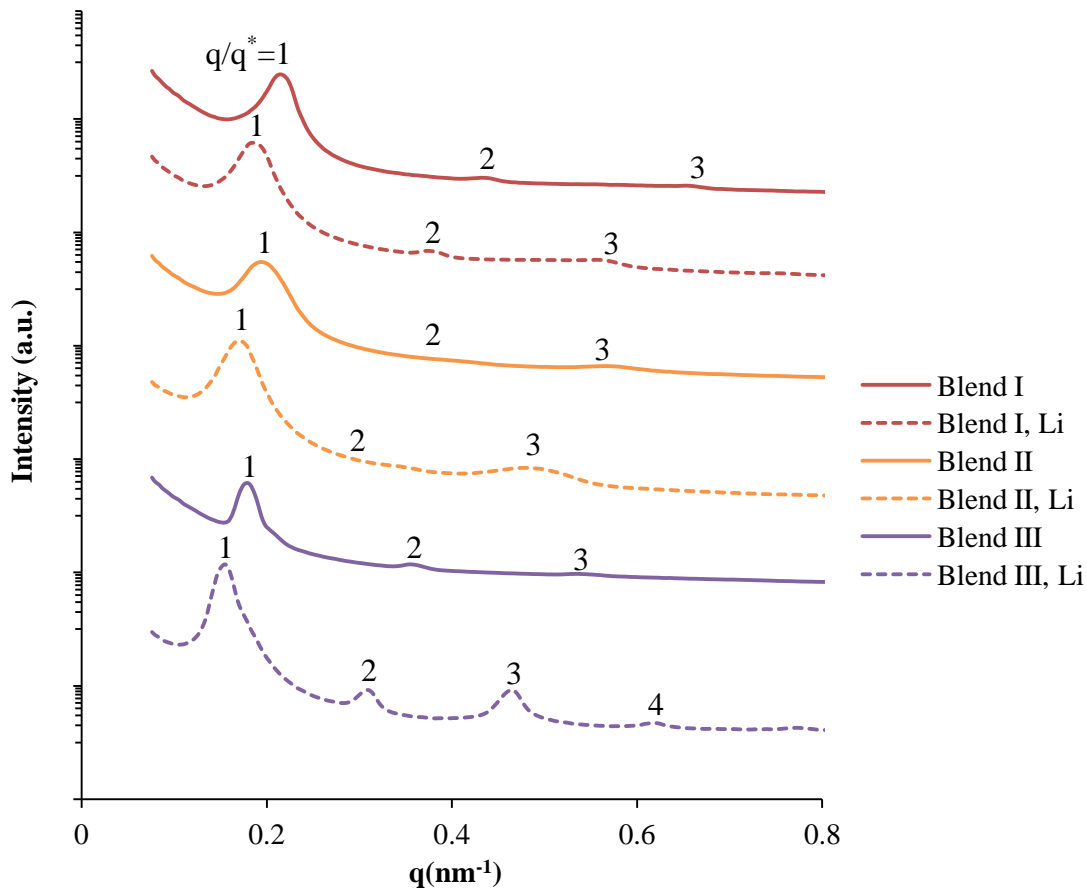


Figure 3.2: SAXS profiles of PS-PEO/PS-POEM copolymer/copolymer blends with and without LiCF_3SO_3 . $[\text{EO}]:[\text{Li}^+]=24:1$. Curves are shifted vertically for clarity.

The domain spacing for each sample as found from the location of the primary peak is given in Table 3.3. The domain spacing for blend I was roughly equivalent to that for PS-PEO indicating that the 20% PS-POEM did not affect the domain spacing. Upon salt doping, blend I had a domain spacing increase of 20%, much smaller than the increase in domain spacing seen for the pure PS-PEO sample. This result may

indicate that the presence of PS-POEM greatly reduced the chain stretching of the PS-PEO component.

The domain spacing was the same for both blend II and blend III. This value was between the values for the domain spacing of pure PS-PEO and PS-POEM, indicating that the increase in PS-POEM percentage from 50% to 80% between the two blends did not affect the domain spacing. Therefore, PS-POEM has a limited ability to stretch the PS-PEO chains. The increase in domain spacing upon salt doping was greater for blend III than for blend II. This result may be due to the increased disorder in blend II. The broad SAXS peaks indicate that the sample is becoming disordered at that composition. Disorder indicates that there is mixing at the interfaces reducing the domain spacing.

Table 3.3: Domain spacing for PS-PEO, PS-POEM, and copolymer/copolymer blends from SAXS data. Spacing is given for both neat and salt doped samples.

| Sample | domain spacing (nm) neat | domain spacing (nm) [EO]:[Li⁺]=24:1 |
|---------------|-------------------------------------|---|
| PS-PEO | 29.3 | 47.8 |
| PS-POEM | 37.7 | 45.3 |
| Blend I | 28.7 | 34.4 |
| Blend II | 33.0 | 35.9 |
| Blend III | 33.0 | 41.6 |

3.1.2 Differential Scanning Calorimetry

DSC heating traces for PS-PEO, PS-POEM, and copolymer/copolymer blends are shown in Figure 3.3. Only the third heating trace is shown. The first trace of each had additional peaks which can be attributed to water evaporation. The second and third traces matched one another.

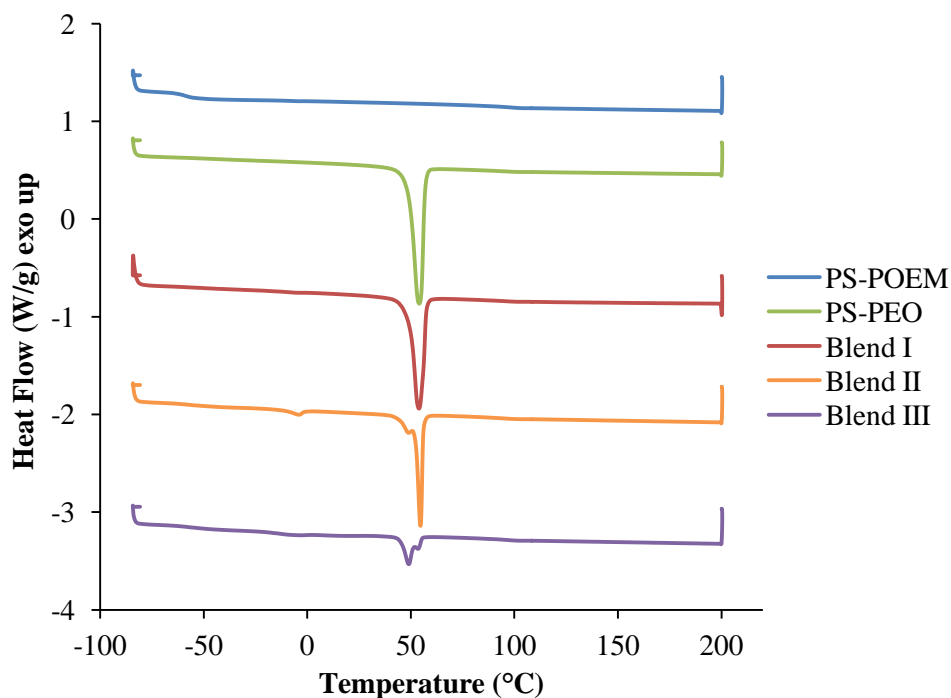


Figure 3.3: DSC traces for PS-PEO, PS-POEM, and copolymer/copolymer blends. The 3rd heating trace is shown with exothermic heat flow up. Samples were heated at a rate of 10 °C/min. Curves shifted vertically for clarity.

PS-POEM showed an increase in heat capacity at -62 °C and at 96 °C corresponding to the glass transitions of the POEM and PS blocks, respectively. PS-POEM showed no melting or crystallization peaks. The PS-PEO sample showed a PS glass transition, and a melting peak at 54 °C associated with the melting of PEO

crystals. No glass transition was distinguishable for PEO indicating that it is highly crystalline.

Blend I showed similar characteristics similar to pure PS-PEO: a PS glass transition and a PEO melting peak. Blend II showed both POEM and PS glass transitions as well as a melting peak at 54 °C. This peak was composed of multiple maxima indicating that the sample crystallized in multiple stages. Blend II also showed an additional small melting peak at -4 °C. It may correspond to additional melting of the PEO block or water in the system. Blend III exhibited similar behavior to blend II but with a smaller melting peak.

The melting temperature, heat of fusion, and percent crystallinity normalized to the weight fraction of the PEO block found from DSC are given in Table 3.4. The heat of fusion was highest for the pure PS-PEO sample and decreased for increasing percentages of PS-POEM. The melting temperature was the same for all samples with the exception of blend III, whose melting peak was at 49 °C. This blend, however, showed a smaller maximum in the melting peak at 54 °C. These results show that the addition of PS-POEM to PS-PEO did not have a significant effect on the melting temperature.

Table 3.4: Melting temperature, heat of fusion, and percent crystallinity for PS-PEO, PS-POEM, and copolymer/copolymer blends as found from DSC.

| Sample | T_m (°C) | ΔH_m (J/g) | Crystallinity (%) |
|---------------|---------------------------|-----------------------------|--------------------------|
| PS-PEO | 54.2 | 50.6 | 58.7 |
| PS-POEM | -- | -- | -- |
| Blend I | 53.9 | 42.5 | 61.6 |
| Blend II | 54.8 | 25.5 | 59.2 |
| Blend III | 49.1 | 9.99 | 57.9 |

The percent crystallinity of the PEO block was the same, within 4%, for all samples, indicating that, although the crystallinity decreased slightly upon PS-POEM addition, it did not significantly inhibit the crystallization of PEO. PEO was able to crystallize around the POEM. However, the addition of PS-POEM did cause the crystal structure to be disrupted as indicated by the multiple melting peaks for blend II and blend III.

The heat of fusion normalized to the mass of PEO is plotted against the weight fraction of PEO in the sample in Figure 3.4. The heat of fusion was constant with respect weight fraction of PEO, indicating that the heat of fusion does not depend on the fraction of PS-POEM.

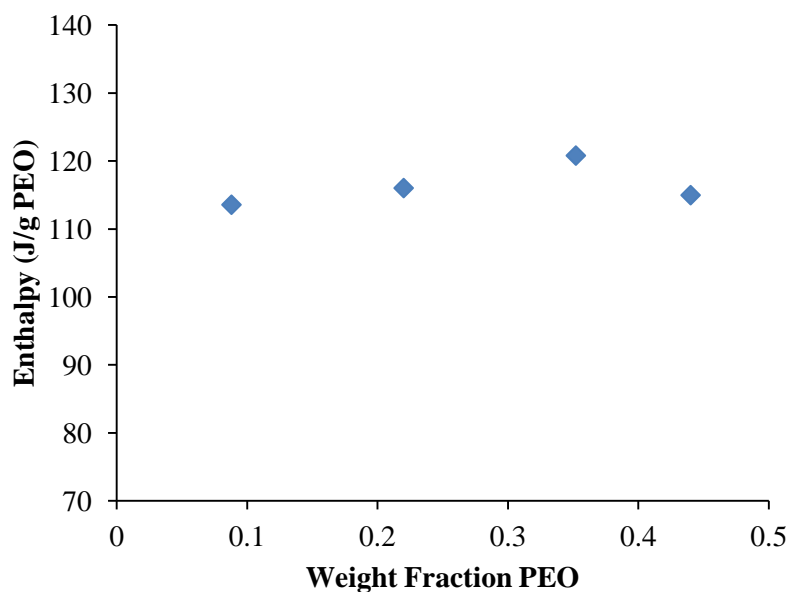


Figure 3.4: Heat of fusion of PS-PEO and copolymer/copolymer blends as found from DSC plotted with respect to the weight fraction of PEO in the sample. Heat of fusion is normalized to the mass of PEO in the sample.

3.1.3 Alternating Current Impedance Spectroscopy

Temperature dependent conductivity data for PS-PEO, PS-POEM, and copolymer/copolymer blends are shown in Figure 3.5. All samples were doped with LiCF_3SO_3 in a 24:1 [EO]: $[\text{Li}^+]$ molar ratio. The conductivity is shown on a logarithmic scale and the absolute temperature is shown on an inverse scale.

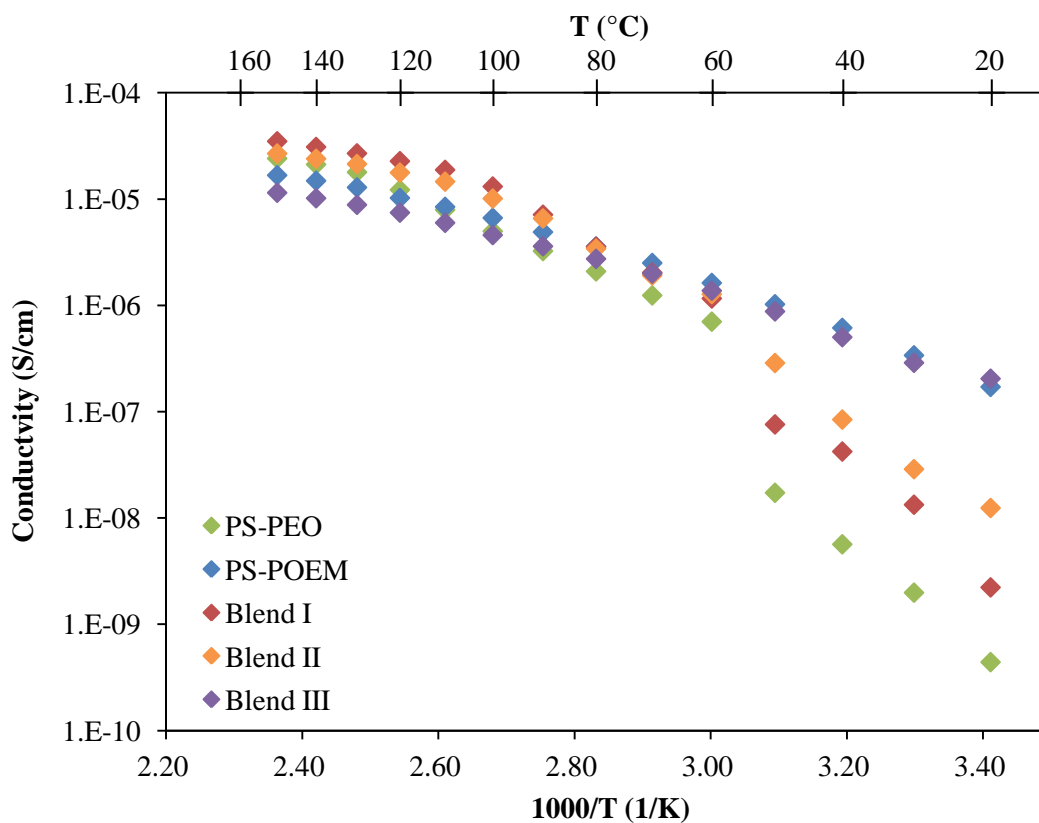


Figure 3.5: Temperature dependent conductivity data for PS-PEO, PS-POEM, and copolymer/copolymer blends. Conductivity is plotted on a logarithmic scale with respect to inverse absolute temperature.

For all samples, the conductivity was higher at higher temperatures. This phenomenon is due to the increased segmental motion of the polymer chains at elevated temperatures. Segmental motion is what promotes lithium ion movement between complex sites, rendering the polymer conductive.

For PS-PEO, there was a discontinuity in conductivity between 50 °C and 60 °C. The discontinuity corresponds to crystallization of the PEO block: PEO crystallizes at 54 °C as shown by DSC. Below the melting temperature, the conductivity of PEO is markedly lower indicating that the amorphous phase is more conductive than the crystalline. After crystallization, lithium ions dissolve into the remaining amorphous regions as they cannot be integrated into the crystalline structure.²¹ Therefore, it is primarily the remaining amorphous regions that contribute to conductivity, leading to the discontinuity.

For PS-POEM, the conductivity decreased as the temperature decreased but there was no discontinuity in the conductivity. The conductivity of PS-POEM was slightly lower than that of PS-PEO for temperatures above 100 °C. Below this temperature PS-POEM was more conductive. The difference in conductivity was largest for temperatures below the melting temperature of PEO due to the fact that POEM remains amorphous whereas PEO crystallizes.

The conductivity profiles of copolymer/copolymer blends were similar to that of the PS-PEO and PS-POEM. Interestingly, at temperatures above 80 °C, blend I had a higher conductivity than either PS-PEO or PS-POEM. The enhancement of conductivity may be due to EO side chains on POEM promoting segmental motion in PS-PEO. Blend I had a sharp decrease in conductivity between 50 and 60 °C due to the crystallization of the PEO block. Below 60 °C, the conductivity of blend I was

between that of PS-PEO and PS-POEM because PS-POEM and PS-PEO in the blend both contribute to the conductivity.

Similar to blend I, blend II had a slightly higher conductivity than either PS-POEM or PS-PEO at temperatures above 80 °C. Below 60 °C, the conductivity of blend II was between that of PS-PEO and PS-POEM, and higher than that of blend I. The conductivity was higher than that of blend I due to the higher PS-POEM content.

The conductivity of blend III was close to that of PS-POEM, albeit slightly lower. There was no sharp drop in conductivity at the melting temperature of PEO indicating that the PS-POEM primarily contributed to the conductivity. The contribution from the PEO block to conductivity was small enough that there was no sharp drop when PEO crystallized.

Temperature dependent conductivity data for PS-PEO, PS-POEM, and copolymer/copolymer blends was fit using the VTF model as shown in Figure 3.6. For PS-PEO, blend I, and blend II, only the data above 60 °C was fit to the VTF model. Below this temperature the samples were largely crystalline as indicated by DSC, and the VTF modeling is applicable only for amorphous materials. For PS-POEM and blend III, the entire temperature range was fit with the VTF model. Two distinct linear regions were seen, corresponding to two different activation energies. One region was above 100 °C and the other was 100 °C and below. The reference temperature was taken to be 227 K. The activation energy and the pre-exponential factor for each sample, found from a least squares fit, are given in Table 3.5.

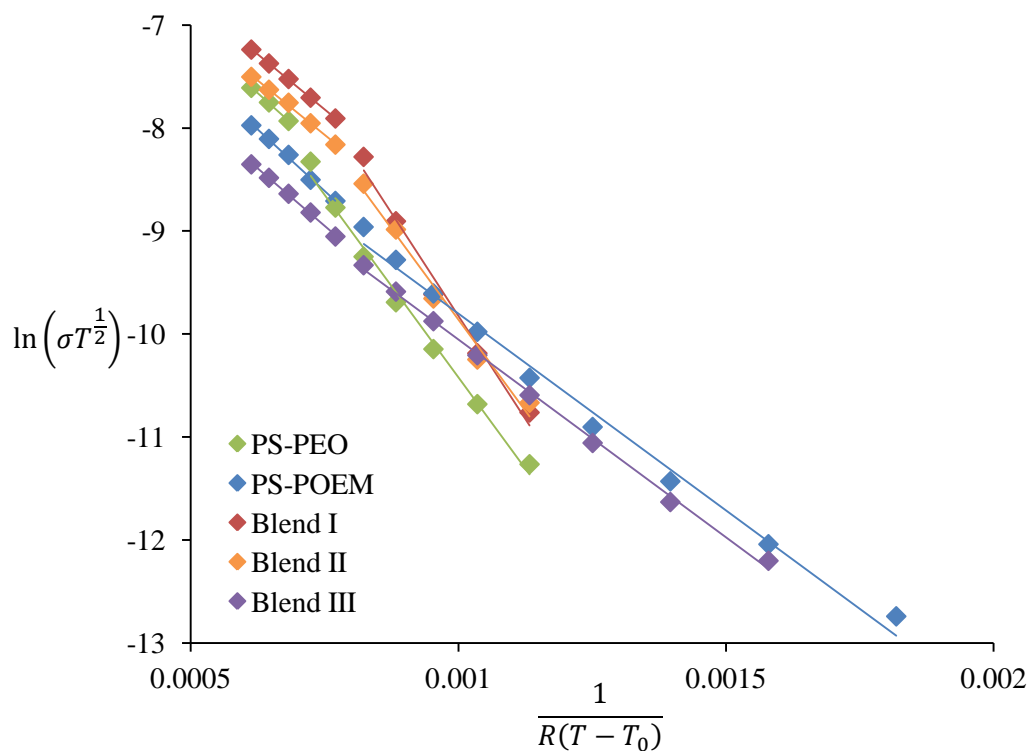


Figure 3.6: Temperature dependent conductivity data for PS-PEO, PS-POEM, and copolymer/copolymer blends fitted to the VTF model. The activation energy was found from the slope and the pre-exponential was found from the y-intercept.

Table 3.5: Activation energy and pre-exponential for PS-PEO, PS-POEM, and copolymer/copolymer blends found from least squares fitting of conductivity data.

| Sample | High temperature | | Low temperature | |
|-----------|----------------------------|------------------------|----------------------------|------------------------|
| | Activation energy (kJ/mol) | Pre-exponential factor | Activation energy (kJ/mol) | Pre-exponential factor |
| PS-PEO | 4.6 ± 0.2 | 0.01 ± 0.1 | 7.1 ± 0.3 | 0.03 ± 0.3 |
| Blend I | 4.26 ± 0.04 | 0.01 ± 0.02 | 8.0 ± 0.6 | 0.2 ± 0.6 |
| Blend II | 4.2 ± 0.2 | 0.007 ± 0.1 | 7.1 ± 0.6 | 0.06 ± 0.6 |
| Blend III | 4.4 ± 0.2 | 0.004 ± 0.08 | 3.84 ± 0.07 | 0.002 ± 0.08 |
| PS-POEM | 4.8 ± 0.2 | 0.007 ± 0.1 | 3.8 ± 0.1 | 0.003 ± 0.2 |

The existence of two distinct regimes is likely due to the glass transition of polystyrene. PS is rubbery above 100 °C and glassy below. The activation energy needed for a lithium ion to move between complexes is dependent upon whether the PEO and/or POEM block is tethered to rubbery or glassy PS. For PS-PEO, blend I, and blend III the activation energy was higher for the glassy PS. This difference is likely due to the increased resistance to chain movement in glassy PS.

Interestingly, the opposite trend was noted for blend III and PS-POEM: the activation energy was higher for rubbery PS. This is likely due to the fact that conduction occurs on the side chains of POEM rather than the backbone. Therefore, glassy PS resisting chain movement of the polymer backbone does not affect activation energy. Furthermore, the rubbery domains cause an increase in the POEM/PS interface size, increasing the activation energy.

In the low temperature regime, the activation energy for PS-POEM was about 30% lower than that for PS-PEO. This result indicates that the energy required for a lithium ion to move between complex sites in PS-POEM is half that required in PS-PEO. This difference is likely due to the fact that the EO side chains on POEM are shorter than the EO backbone of linear PEO; therefore, require less energy to move.

In the high temperature regimes, the activation energy for all three blends was close to that of PS-POEM. This indicates that PS-POEM has a much larger contribution to activation energy than PS-PEO. The greater contribution is likely due to the greater number of complex sites available in PS-PEO than are available in PS-POEM. In the low temperature regimes, the activation energy of blend III was close to that of PS-POEM, whereas the activation energies of blend I and blend III were close to that of PS-PEO.

The pre-exponential did not show a consistent trend as the activation energy did. In general, the higher PS-PEO content samples had a larger pre-exponential factor indicating that there are a greater number of charge carriers in these samples. The greater number of charge carriers are due to the fact that the entire backbone of PEO provides complex sites, whereas complex formation occurs only on the side chains of POEM leading to more charge carriers in PEO than in POEM.

3.1.4 Conclusions

Copolymer/copolymer blends were made with PS-PEO and PS-POEM to enhance the conductivity. Three copolymer/copolymer blends were made. SAXS studies showed that the PS-PEO, PS-POEM, and copolymer/copolymer blends all had lamellar morphology. The domain spacing increased upon salt doping, indicating that the lithium ions formed complexes with the PEO block of PS-PEO and the EO side chains on the POEM block of PS-POEM. DSC studies showed that the percent crystallinity normalized to the PEO block was the same for all samples, indicating that the presence of POEM did not prevent crystallization. AC impedance studies showed that the conductivity of PS-PEO decreased markedly below the melting temperature indicating that conduction occurs preferentially in the amorphous phase. Blend I and blend III also showed a sharp decrease in conductivity further indicating that the addition of PS-POEM did not successfully prevent crystallization. Below 60 °C, PS-POEM showed the highest conductivity indicating that it may be better candidate for lithium ion battery applications than PS-PEO. Furthermore, PS-POEM had a smaller activation energy for lithium ion movement than PS-PEO, although it also showed a smaller pre-exponential indicating fewer charge carriers.

3.2 Nanoparticle Additives

The second method employed in this work to enhance the conductivity of block copolymer electrolytes was the addition of titania nanoparticles. The triblock copolymer PS-PEO-PS was used for this study. The molecular weight was 41,000 g/mol and the weight percent PEO was 78.

The triblock copolymer PS-PEO-PS has advantages over PS-PEO. ABA type copolymers exhibit higher mechanical strength than their AB type analogs.²² Furthermore, the crystallinity of the PEO block is thought to be decreased in ABA type copolymers due to the increased tethering of PEO to PS around the interface.²³

The addition of titania nanoparticles has been shown to increase the conductivity of polymer electrolytes.^{24,25,26,27} Nanoparticles with large surface areas are thought to prevent PEO chain reorganization thus promoting amorphous regions and increasing the ionic conductivity. However, the aggregation of nanoparticles must be prevented to realize this benefit. Different techniques have been used in literature to prevent aggregation such as high energy ball milling^{24,25} and the addition of a ligand to the particles.^{28,29} Some studies, however, have shown that the conductivity of PS-PEO decreases upon the addition of titania nanoparticles.³⁰ More work needs to be done to determine how nanoparticle addition effects conductivity.

For this study, 18 nm titania nanoparticles coated in an oleic acid ligand were used. Oleic acid, shown in Figure 3.7, is an 18-carbon monounsaturated fatty acid. The hydrophobic chains are thought to prevent titania particles from agglomerating via steric hindrance. A series of PS-PEO-PS samples were made with ethylene oxide to titania mass ratios of 5:1, 10:1, and 20:1.

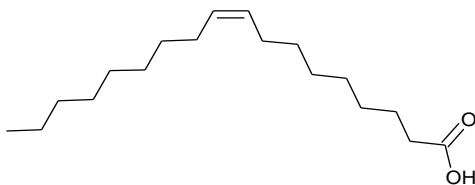


Figure 3.7: Structure of oleic acid ligand bound to TiO_2 nanoparticles.

3.2.1 Transmission Electron Microscopy

TEM images of the titania nanoparticles used are shown in Figure 3.8. The particles are slightly elongated spheres with an average diameter of 18 nm.

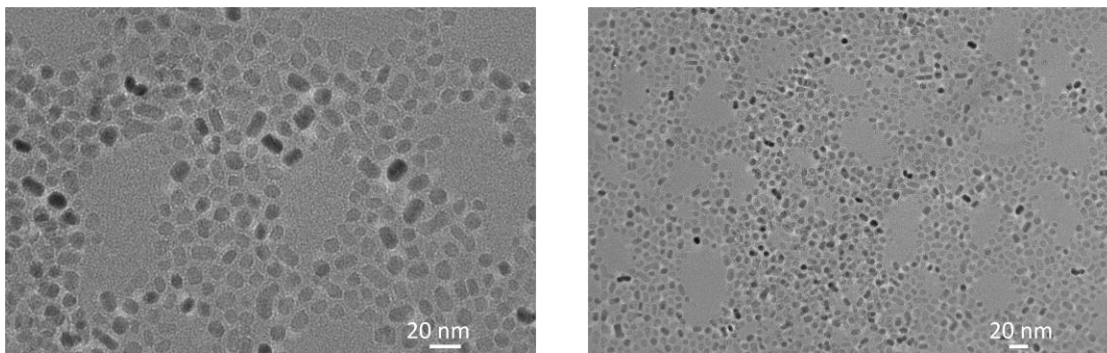


Figure 3.8: TEM images of oleic acid coated TiO_2 nanoparticles.

TEM studies were done on a PS-PEO-PS, TiO_2 sample to determine the dispersion of the nanoparticles within the polymer matrix shown in Figure 3.9. The titania composition was 10:1 EO: TiO_2 mass ratio. TEM images were taken with no staining.

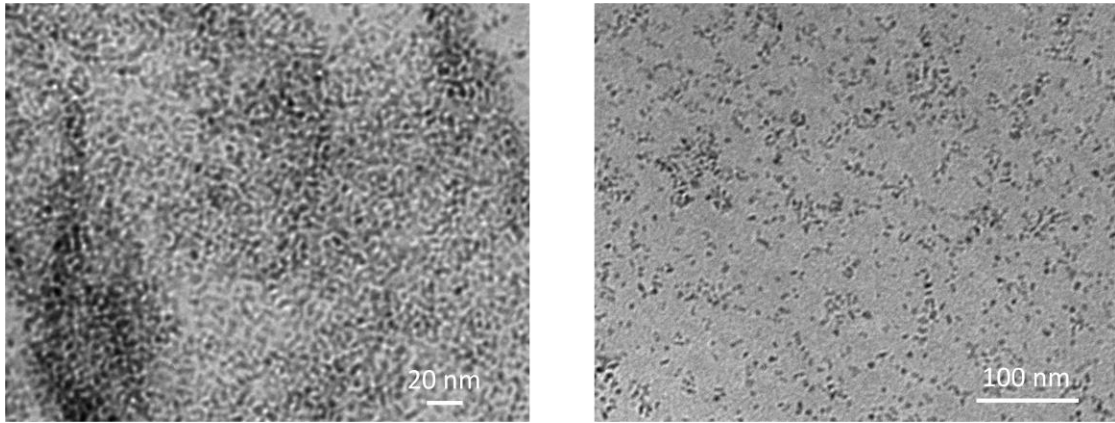


Figure 3.9: TEM images of TiO_2 nanoparticles dispersed in the PS-PEO-PS matrix.

The TEM images show that the titania nanoparticles are well dispersed in the polymer matrix. The nanoparticles did not agglomerate upon mixing nor did they show a change in size or shape.

3.2.2 Differential Scanning Calorimetry

DSC heating traces for PS-PEO-PS doped with LiCF_3SO_3 and varying amounts of titania are shown in Figure 3.10. Only the third heating trace is shown. The first trace of each had additional peaks which can be attributed to water evaporation. The second and third traces matched one another.

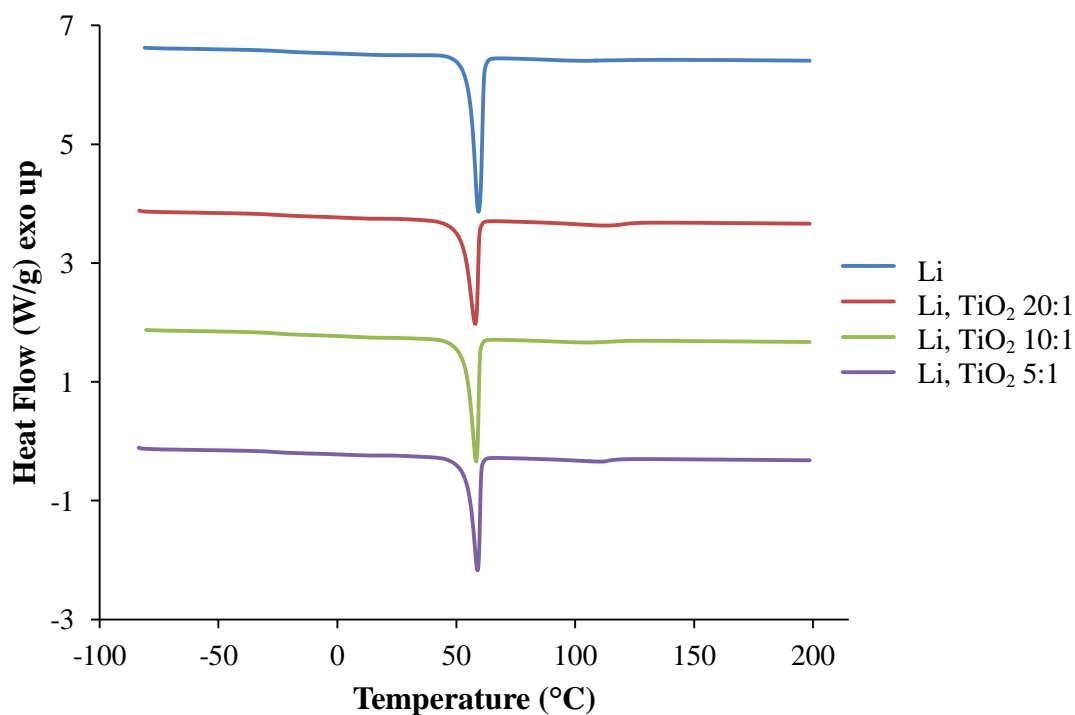


Figure 3.10: DSC traces for PS-PEO-PS doped with LiCF_3SO_3 and varying amounts of titania. For all samples $[\text{EO}]:[\text{Li}^+]=24:1$. Titania compositions are given as EO to TiO_2 mass ratios. The 3rd heating trace is shown with exothermic heat flow up. Samples were heated at a rate of 10 °C/min. Curves shifted vertically for clarity.

All of the traces showed a first order phase change around 60 °C corresponding to the melting temperature of the PEO block. No glass transitions were

discernible from DSC. The melting temperature, heat of fusion, and percent crystallinity normalized to the weight fraction of the PEO block are given in Table 3.7.

Table 3.7: Melting temperature, heat of fusion, and percent crystallinity for PS-PEO-PS, LiCF₃SO₃, TiO₂ samples as found from DSC. For all samples [EO]:[Li⁺]=24:1. Titania compositions are given as EO:TiO₂ mass ratios.

| Sample | T _m (°C) | ΔH _m (J/g) | Crystallinity (%) |
|--------------------------------------|---------------------|-----------------------|-------------------|
| PS-PEO-PS, Li | 59.4 | 75.0 | 54.7 |
| PS-PEO-PS, Li, TiO ₂ 20:1 | 57.9 | 57.8 | 43.6 |
| PS-PEO-PS, Li, TiO ₂ 10:1 | 58.9 | 59.6 | 46.5 |
| PS-PEO-PS, Li, TiO ₂ 5:1 | 58.8 | 54.7 | 45.4 |

The melting temperature was the same, within 2 °C, for all samples indicating that the addition of nanoparticles did not affect the melting temperature of PEO. The addition of titania nanoparticles did, however, result in a decrease in percent crystallinity of the PEO block. This decrease is likely due to the nanoparticles interacting with the PEO block preventing chain reorganization thus promoting amorphous regions. Interestingly, the percent crystallinity was within 3% for all three titania doping ratios, indicating that the changes in titania composition did not lead to changes in crystallinity. These data may indicate an upper limit on the amount of titania that is able to dissolve into the PEO block. It also may indicate that agglomeration of titania particles occurred at higher doping ratios limiting its effect on crystallinity.

In addition to the PEO melting peak around 60 °C, another, smaller, first order phase transition was seen around 115 °C as shown in Figure 3.11.

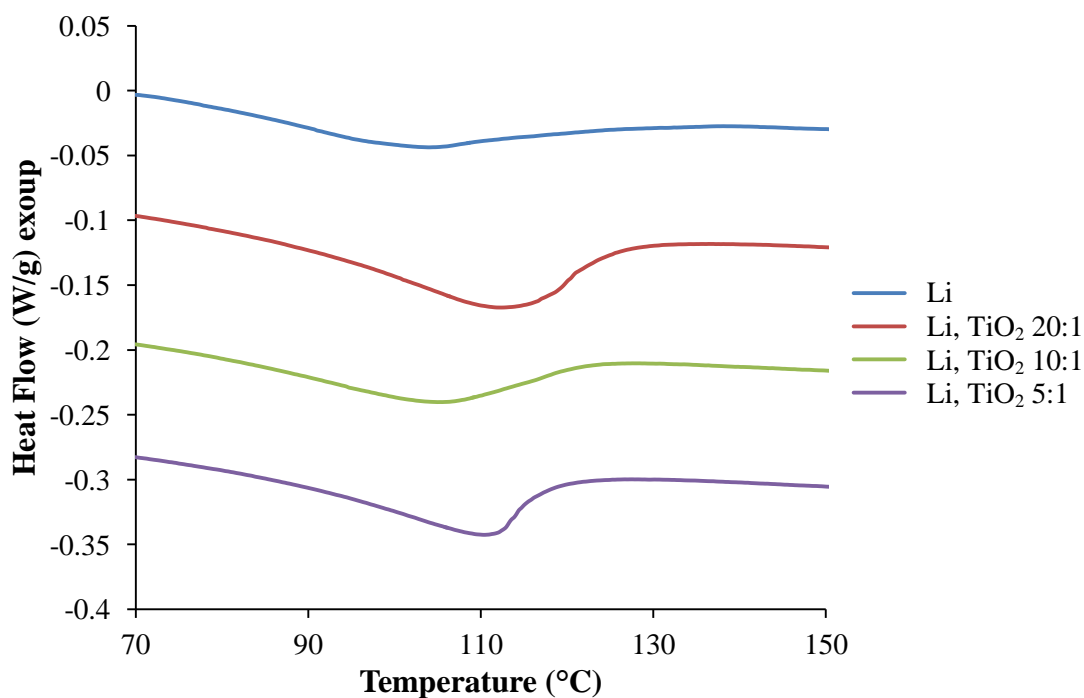


Figure 3.11: Zoom in around 115 °C of DSC traces for PS-PEO-PS doped with LiCF₃SO₃ and varying amounts of titania. Curves shifted vertically for clarity.

These peaks may be associated with the melting of ethylene oxide lithium ion complexes. This transition is indicated on the phase diagram developed by Robitaille and Fauteux shown in Figure 3.12.⁵ At this temperature, the lithium ion/ethylene oxide complexes dissociate to form a single liquid phase.

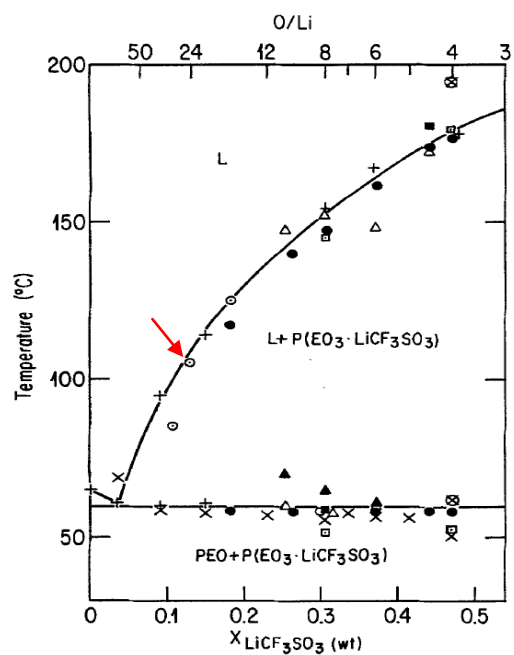


Figure 3.12: PEO, LiCF₃SO₃ phase diagram adapted from ref. 5. Copyright 2003 The Electrochemical Society. Arrow represents salt composition used in this work.

3.2.3 Alternating Current Impedance Spectroscopy

Temperature dependent conductivity data for PS-PEO-PS samples are shown in Figure 3.13. All samples were doped with LiCF_3SO_3 in a 24:1 $[\text{EO}]:[\text{Li}^+]$ molar ratio. The conductivity is shown on a logarithmic scale and the absolute temperature is shown on an inverse scale.

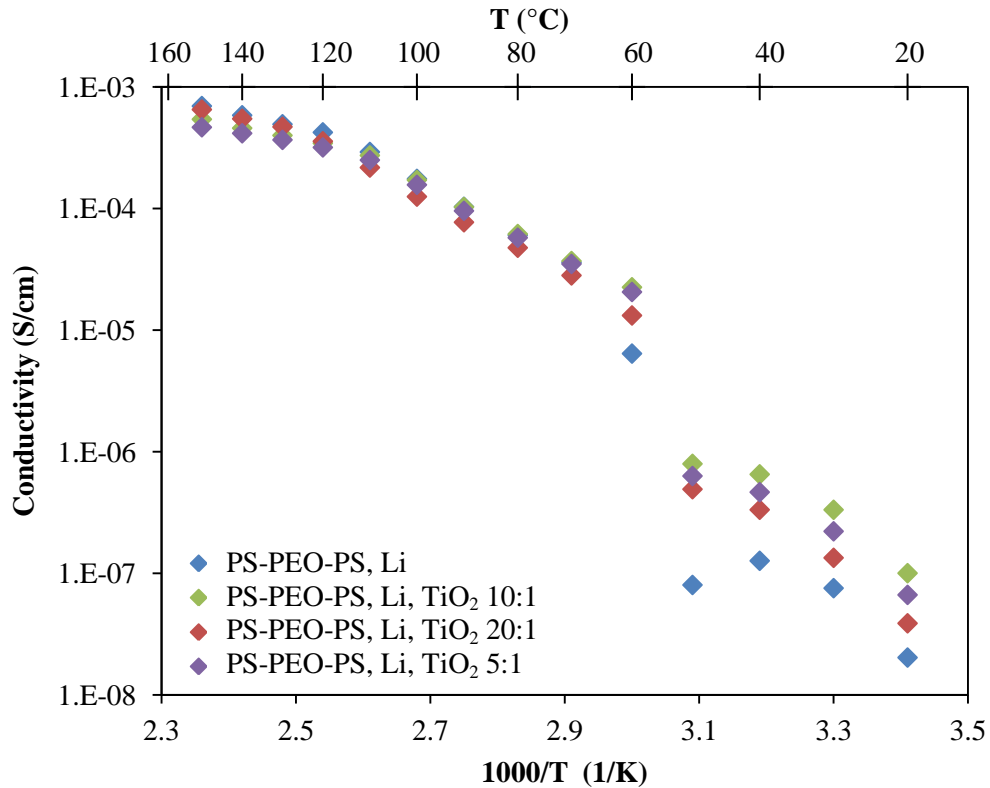


Figure 3.13: Temperature dependent conductivity data for PS-PEO-PS doped with LiCF_3SO_3 and varying amounts of titania. Conductivity is plotted on a logarithmic scale with respect to inverse absolute temperature.

Similar to what was seen in the copolymer/copolymer blends study, the conductivity of all samples was higher at higher temperatures. This phenomenon is due to the increased segmental motion of the polymer chains at elevated temperatures.

Also, there was a discontinuity in conductivity between 50 and 60 °C corresponding to crystallization of the PEO block: The PEO block crystallizes at 58 °C as shown by DSC. Below the melting temperature, the conductivity is markedly lower because conduction occurs primarily in the amorphous phase. For the PS-PEO-PS sample, the conductivity at 50 °C was lower than the conductivity at 60 °C. This data may be indicative of error. The sample may not have reached the correct temperature.

Below 60 °C, the conductivity of PS-PEO-PS increased upon addition of titania. An increase was seen for all titania doping ratios due to the reduction in crystallization of the PEO block. However, the increase in conductivity did not scale with titania composition. The highest increase was seen for a doping ratio of 10:1, followed 5:1, then 20:1. This result is interesting and may be due to the interaction between titania and the lithium salt. It is likely that, in addition to preventing crystallization, the presence of titania nanoparticles promoted conduction of lithium ions. This effect caused the lowest conductivity to be seen for the lowest doping ratio, 20:1. The fact that the 5:1 doping ratio showed a lower conductivity than 10:1 may be due to agglomeration of titania nanoparticles at this doping ratio.

Temperature dependent conductivity data for PS-PEO-PS and titania doped samples was fit using the VTF model as shown in Figure 3.14. Only the data above 60 °C was fit to the VTF model. Below this temperature the samples were largely crystalline as indicated by DSC, and the VTF modeling is applicable only for amorphous materials. Two distinct linear regions were seen, corresponding to two different activation energies. One region was 100 °C and above and the other was below 100 °C. The reference temperature was taken to be 227 K. The activation

energy and the pre-exponential factor for each sample, found from a least squares fit, are given in Table 3.8.

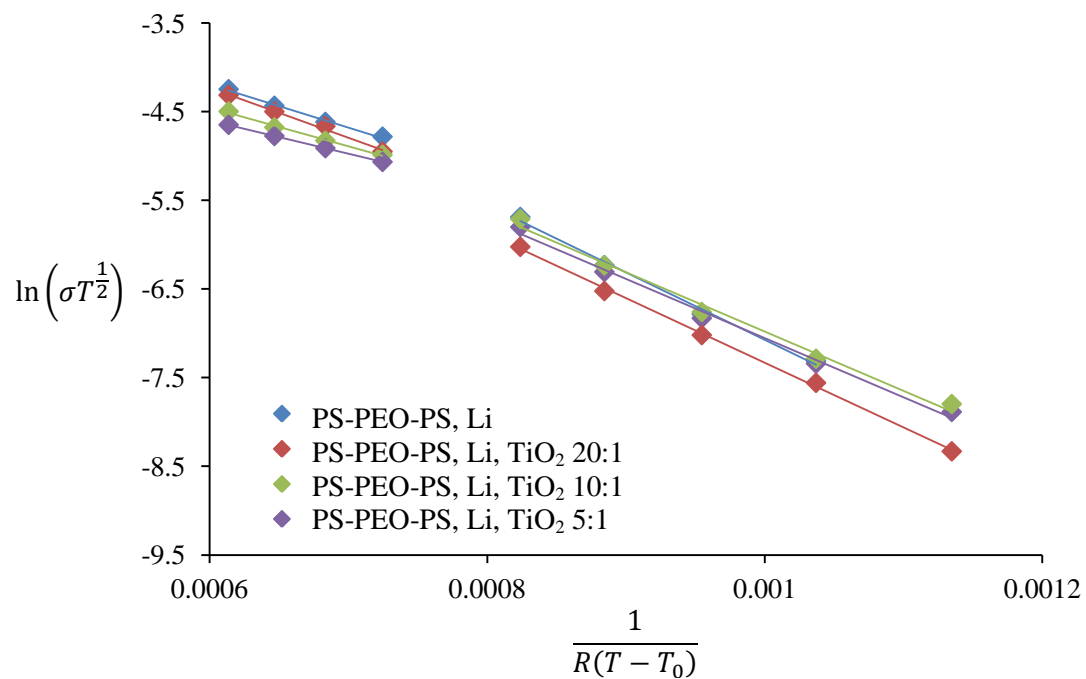


Figure 3.14: Temperature dependent conductivity data for PS-PEO-PS and titania doped samples fitted to the VTF model. The activation energy was found from the slope and the pre-exponential was found from the y-intercept.

Table 3.8: Activation energy and pre-exponential for PS-PEO-PS and titania doped samples found from least squares fitting of conductivity data.

| Sample | High temperature | | Low temperature | |
|--------------------------------------|----------------------------|------------------------|----------------------------|------------------------|
| | Activation Energy (kJ/mol) | Pre-exponential factor | Activation Energy (kJ/mol) | Pre-exponential factor |
| PS-PEO-PS, Li | 4.8 ± 0.3 | 0.3 ± 0.2 | 8.1 ± 0.4 | 2.7 ± 0.4 |
| PS-PEO-PS, Li, TiO ₂ 20:1 | 5.6 ± 0.3 | 0.4 ± 0.2 | 7.7 ± 0.3 | 1.4 ± 0.3 |
| PS-PEO-PS, Li, TiO ₂ 10:1 | 4.4 ± 0.3 | 0.2 ± 0.2 | 7.1 ± 0.4 | 1.1 ± 0.4 |
| PS-PEO-PS, Li, TiO ₂ 5:1 | 3.77 ± 0.01 | 0.097 ± 0.007 | 7.0 ± 0.3 | 1.0 ± 0.3 |

As noted in the blends study, the existence of two distinct regimes was likely due to the glass transition of polystyrene. The activation energy for each sample was higher for the glassy PS. This difference is likely due to the increased resistance to chain movement in glassy PS. With the exception of PS-PEO-PS in the high temperature regime, the activation energy decreased for increasing amounts of titania. This trend indicates that the titania nanoparticles facilitated the transport of lithium ions through the polymer matrix. The pre-exponential factor also decreased for increasing amounts of titania. Values for the titania doped samples were much lower than that for the non doped sample. This result indicates that there are a greater number of charge carriers in the non doped sample.

To determine whether the increase in conductivity upon nanoparticles addition was solely due to suppression of crystallization, PS-POEM was doped with titania. POEM is an amorphous material; therefore, there is no benefit from the suppression of crystallization by titania. Temperature dependent conductivity data for PS-POEM

samples are shown Figure 3.15. Both samples were doped with LiCF_3SO_3 in a 24:1 $[\text{EO}]:[\text{Li}^+]$ molar ratio. The titania doped sample had 10 to 1 $\text{EO}:\text{TiO}_2$ mass ratio.

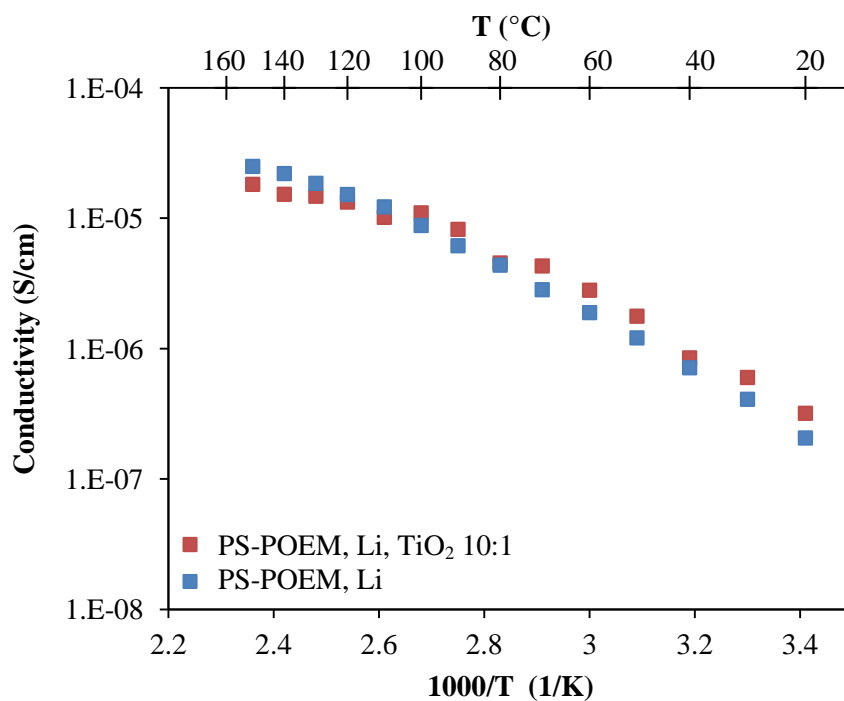


Figure 3.15: Temperature dependent conductivity data for PS-POEM doped with LiCF_3SO_3 with and without titania. Conductivity is plotted on a logarithmic scale with respect to inverse absolute temperature.

Above 100 °C, the conductivity of the non titania doped sample was slightly lower, and below 100 °C, the opposite was true. These data indicates that titania nanoparticles do promote lithium ion conduction below 100 °C, implying that the oleic coated nanoparticles are themselves, conductive for lithium ions. However, there exist no previously proposed mechanisms for this phenomenon. More work

could be done to maximize the conductivity of PEO based polymers via titania nanoparticles doping.

3.2.4 Conclusions

Titania nanoparticles coated in an oleic acid ligand were added to the triblock copolymer PS-PEO-PS to enhance the conductivity. Three titania doped samples were made with EO:TiO₂ mass ratios of 20:1, 10:1, and 5:1. DSC studies showed that addition of titania nanoparticles decreased the crystallinity of the PEO block by 10%. This reduction was independent of the doping ratio, indicating that there is an upper limit on the amount of titania able to dissolve into the PEO block, possibly due to the agglomeration of the nanoparticles. AC impedance studies showed that the conductivity of titania doped samples and non doped PS-PEO-PS were equal above the crystallization temperature of PEO. Below the crystallization temperature, the titania doped sample had a significantly larger conductivity. The highest conductivity was seen for the 10:1 titania doped sample, followed by 5:1, then 20:1. This result shows that it is likely that, in addition to preventing crystallization, titania nanoparticles promote conduction of lithium ions.

Chapter 4

THESIS SUMMARY AND RECOMMENDATIONS FOR FUTURE WORK

4.1 Copolymer/Copolymer Blends

To enhance the conductivity of PS-PEO, copolymer/copolymer blends were made with PS-POEM. PS-PEO, PS-POEM, and copolymer/copolymer blends all had lamellar morphology, and the domain spacing increased upon salt doping indicating that the lithium ions formed complexes with the ethylene oxide groups. The percent crystallinity of the PEO block was the same for all samples indicating that the presence of POEM did not prevent crystallization. The conductivity of PS-PEO, and copolymer/copolymer blends decreased markedly below the melting temperature of PEO (60 °C) as conduction occurs preferentially in the amorphous phase. Below 60 °C, PS-POEM showed the highest conductivity indicating that it may be better candidate for lithium ion battery applications than PS-PEO.

4.2 Nanoparticle Additives

The second strategy employed to enhance the conductivity was the addition of titania nanoparticles. Three titania doped samples were made with EO:TiO₂ mass ratios of 20:1, 10:1, and 5:1. The addition of titania nanoparticles decreased the crystallinity of the PEO block by 10% independent of the doping ratio. The conductivity of titania doped samples and non doped PS-PEO-PS were equal above the crystallization temperature of PEO (60 °C). Below the crystallization temperature, the titania doped sample had a significantly larger conductivity. The highest

conductivity was seen for the 10:1 titania doped sample, followed by 5:1 then 20:1. This result shows that it is likely that, in addition to preventing crystallization, titania nanoparticles promoted conduction of lithium ions.

4.3 Recommendations for Future Work

The copolymer/copolymer blends study shown in the first half of this thesis indicated that PS-POEM is a promising candidate for lithium ion battery membranes. PS-POEM does not crystallize and therefore does not show a sharp drop in crystallization seen in systems containing PS-PEO. Furthermore, the conductivity of PS-PEOM is three orders of magnitude higher than that of PS-PEO at room temperature. Further studies need to be done to further enhance the conductivity of PS-POEM to be commercially viable.

It also may be possible to further enhance the conductivity of PS-PEO. If the crystallization of PEO is fully inhibited, then the conductivity of PS-PEO may be high enough for commercial applications. Further studies need to be done to inhibit crystallization using nanoparticles. One possibility is to reduce the doping ratio of titania nanoparticles. As no change in crystallinity was seen between doping ratios, there may be a minimum crystallinity corresponding to a lower doping ratio. Another possibility is for nanoparticles to be coated in an ion conducting ligand, or with hydrophilic ligands that interact more strongly with PEO. Furthermore, the size of the nanoparticles can be adjusted to better match the length scale of polymer crystals.

With further work, lithium and lithium ion batteries can be commercialized using polymeric materials for the membrane. Polymer membranes will greatly increase the safety of devices that rely on lithium batteries such as electric vehicles and consumer electronics.

REFERENCES

- ¹ Armand, M. and Tarascon, J.M. *Nature*. **2001**, *414*, 359-367.
- ² Young, Wen-Shiue. Multi-Component Block Copolymer Electrolytes for Solid-State Lithium Batteries. Ph.D. Thesis, University of Delaware, Spring 2012.
- ³ Brandt, K. *Solid State Ionics*. **1994**, *69*, 173-183.
- ⁴ Hallinan Jr., D.T. and Balsara, N.P. *Annual Review of Materials Research*. **2013**, *43*, 503-523.
- ⁵ Robitaille, C.D. and Fauteux, D. *Journal of the Electrochemical Society*. **1986**, *133*, (2), 315-325.
- ⁶ Meyer, W. H. *Advanced Materials*. **1998**, *10*, (6), 439-448.
- ⁷ Agrawal, R.C., and Pandey, G.P. *Journal of Physics D: Applied Physics*. **2008**, *41*, 223001-223019.
- ⁸ Young, W.S. et al. *Journal of Polymer Science Part B: Polymer Physics*. **2013**, *52*, 1-16.
- ⁹ Bates, F.S. *Science*. **1991**, *251*, (4996), 898-905.
- ¹⁰ Matsen, M.W. *Macromolecules*. **2012**, *45*, (4), 2162-2165.
- ¹¹ Mai, YY et al. *Chemical Society Reviews*. **2012**, *41*, (18), 5969-5985.
- ¹² Tureau, M.S. and Epps III, T.H. *Macromolecules*, **2012**, *445*, (20), 8347-8355.
- ¹³ Young, W.S. and Epps III, T.H. *Macromolecules*. **2012**, *45*, 4689-4697.
- ¹⁴ Kobayashi, N. et al. *Journal of Physical Chemistry*. **1985**, *89*, 987-991.
- ¹⁵ Ahn, J.H., et al. *Journal of Power Sources*. **2003**, *119-121*, 422-426.
- ¹⁶ Fairclough, J.P.A, et al. *Radiation Physics and Chemistry*. **1999**, *56*, (1-2), 159-173.

- ¹⁷ "Differential Scanning Calorimetry." The University of Southern Mississippi, **2005**.
- ¹⁸ Masoud, E.M., et al. *Journal of Alloys and Compounds*. **2013**, 575, 223-228.
- ¹⁹ Ohno, Hiroyuki, et al. *Solid State Ionics*. **1993**, 62, 257-264.
- ²⁰ Epps, III, T.H., et al. *Chemistry of Materials*. **2002**, 14, (4), 1706-1714.
- ²¹ Berthier, C. et al. *Solid State Ionics*. **1983**, 11, 91-95.
- ²² Sasaki, M. et al. *Journal of Applied Polymer Science*. **2010**, 118, (3), 1766-1773.
- ²³ Weimann, P.A. et al. *Journal of Polymer Science Part B: Polymer Physics*. **1999**, 37, (16), 2053-2068.
- ²⁴ Liu, H.K. et al. *Journal of New Materials for Electrochemical Systems*. **2007**, 10, 101-104.
- ²⁵ Ahn, J.-H. et al. *Journal of Power Sources*. **2003**, 119-121, 422-426.
- ²⁶ Croce, F. et al. *Letters to Nature*. **1998**, 394, 456-458.
- ²⁷ Mohamed Ali, T. et al. *Ionics*. **2013**, 19, 1115-1123.
- ²⁸ Lin, J.-F. et al. *Applied Materials and Interfaces*. **2013**, 5, 1009-1016.
- ²⁹ Lin, Y.-Y. et al. *Applied Physics Letters*, **2008**, 92, 053312.
- ³⁰ Gurevitch, I. et al. *Journal of the Electrochemical Society*. **2013**, 160, (9), A1611-A1617.

Appendix

COPYRIGHT PERMISSIONS

| | |
|---|---|
| License Number | 3362560243987 |
| License date | Apr 05, 2014 |
| Licensed content publisher | Nature Publishing Group |
| Licensed content publication | Nature |
| Licensed content title | Issues and challenges facing rechargeable lithium batteries |
| Licensed content author | J.-M. Tarascon and M. Armand |
| Licensed content date | Nov 15, 2001 |
| Type of Use | reuse in a dissertation / thesis |
| Volume number | 414 |
| Issue number | 6861 |
| Requestor type | academic/educational |
| Format | electronic |
| Portion | figures/tables/illustrations |
| Number of figures/tables /illustrations | 1 |
| Figures | Figure 1 |
| Author of this NPG article | no |
| Your reference number | None |
| Title of your thesis / dissertation | Enhanced Conductivity of Block Copolymer Electrolytes for Lithium Batteries |
| Expected completion date | May 2014 |
| Estimated size (number of pages) | 60 |
| Total | 0.00 USD |

Figure A.1: Copyright permission for Figure 1.1, battery energy densities.

| | |
|---------------------------------------|---|
| License Number | 3362561016673 |
| License date | Apr 05, 2014 |
| Licensed content publisher | John Wiley and Sons |
| Licensed content publication | Journal of Polymer Science Part B: Polymer Physics |
| Licensed content title | Block copolymer electrolytes for rechargeable lithium batteries |
| Licensed copyright line | Copyright © 2013 Wiley Periodicals, Inc. |
| Licensed content author | Wen-Shiue Young,Wei-Fan Kuan,Thomas H. Epps, |
| Licensed content date | Nov 4, 2013 |
| Start page | 1 |
| End page | 16 |
| Type of use | Dissertation/Thesis |
| Requestor type | University/Academic |
| Format | Electronic |
| Portion | Figure/table |
| Number of figures/tables | 1 |
| Original Wiley figure/table number(s) | Figure 1 |
| Will you be translating? | No |
| Title of your thesis / dissertation | Enhanced Conductivity of Block Copolymer Electrolytes for Lithium Batteries |
| Expected completion date | May 2014 |
| Expected size (number of pages) | 60 |
| Total | 0.00 USD |

Figure A.2: Copyright permission for Figure 1.2, lithium ion battery operation.

| | |
|---------------------------------------|---|
| License Number | 3362580482196 |
| License date | Apr 05, 2014 |
| Licensed content publisher | John Wiley and Sons |
| Licensed content publication | Advanced Materials |
| Licensed content title | Polymer Electrolytes for Lithium-Ion Batteries |
| Licensed copyright line | © 1998 WILEY-VCH Verlag GmbH, Weinheim, Fed. Rep. of Germany |
| Licensed content author | Wolfgang H. Meyer |
| Licensed content date | Jan 26, 1999 |
| Start page | 439 |
| End page | 448 |
| Type of use | Dissertation/Thesis |
| Requestor type | University/Academic |
| Format | Electronic |
| Portion | Figure/table |
| Number of figures/tables | 1 |
| Original Wiley figure/table number(s) | Figure 2 |
| Will you be translating? | No |
| Title of your thesis / dissertation | Enhanced Conductivity of Block Copolymer Electrolytes for Lithium Batteries |
| Expected completion date | May 2014 |
| Expected size (number of pages) | 60 |
| Total | 0.00 USD |

Figure A.3: Copyright permission for Figure 1.3, Movement of lithium ions through polymer system.



RightsLink®

Home

Account
Info

Help



ACS Publications
High quality. High impact.

Title: Effect of Architecture on the
Phase Behavior of AB-Type
Block Copolymer Melts

Author: M. W. Matsen

Publication: Macromolecules

Publisher: American Chemical Society

Date: Feb 1, 2012

Copyright © 2012, American Chemical Society

Logged in as:

Ellen Reed

Account #:
3000774053

LOGOUT

PERMISSION/LICENSE IS GRANTED FOR YOUR ORDER AT NO CHARGE

This type of permission/license, instead of the standard Terms & Conditions, is sent to you because no fee is being charged for your order. Please note the following:

- Permission is granted for your request in both print and electronic formats, and translations.
- If figures and/or tables were requested, they may be adapted or used in part.
- Please print this page for your records and send a copy of it to your publisher/graduate school.
- Appropriate credit for the requested material should be given as follows: "Reprinted (adapted) with permission from (COMPLETE REFERENCE CITATION). Copyright (YEAR) American Chemical Society." Insert appropriate information in place of the capitalized words.
- One-time permission is granted only for the use specified in your request. No additional uses are granted (such as derivative works or other editions). For any other uses, please submit a new request.

If credit is given to another source for the material you requested, permission must be obtained from that source.

Figure A.4: Copyright permission for Figure 1.4, block copolymer phase diagram.

| | |
|----------------------------------|---|
| License Number | 3362590960093 |
| License date | Apr 05, 2014 |
| Licensed content publisher | Royal Society of Chemistry |
| Licensed content publication | Chemical Society Reviews |
| Licensed content title | Self-assembly of block copolymers |
| Licensed content author | Yiyong Mai,Adi Eisenberg |
| Licensed content date | Jul 9, 2012 |
| Volume number | 41 |
| Issue number | 18 |
| Type of Use | Thesis/Dissertation |
| Requestor type | academic/educational |
| Portion | figures/tables/images |
| Number of figures/tables/images | 1 |
| Distribution quantity | 20 |
| Format | electronic |
| Will you be translating? | no |
| Order reference number | None |
| Title of the thesis/dissertation | Enhanced Conductivity of Block Copolymer Electrolytes for Lithium Batteries |
| Expected completion date | May 2014 |
| Estimated size | 60 |
| Total | 0.00 USD |

Figure A.5: Copyright permission for Figure 1.4, block copolymer morphologies.

Request for Permission to Reproduce or Re-Publish ECS Material

Please fax this form to: The Electrochemical Society (ECS), Attn: Permissions Requests, 1.609.730.0629.
You may also e-mail your request to: copyright@electrochem.org. Include all the information as required on this form. Please allow 3-7 days for your request to be processed.

I am preparing a (choose one): paper chapter book thesis

entitled: Enhanced Conductivity of Block Copolymer Electrolytes for Lithium Batteries

to be published by: University of Delaware

in an upcoming publication entitled: N/A

I request permission to use the following material in the publication noted above, and request nonexclusive rights for all subsequent editions and in all foreign language translations for distribution throughout the world.

Description of material to be used—Indicate what material you wish to use (figures, tables, text, etc.) and give the full bibliographic reference for the source publication. You may attach a separate list, organized by ECS title.

Phase Diagrams and Conductivity characterization of

Some PEO-LiX Electrolytes. J. Electrochem. Soc. 1986

Volume 133, issue 2, 315-325 C.D. Raboinville and

D. Fauteux

Figure 1

Signature: Ellen H. Reed Date: April 8, 2014

Name: Ellen H. Reed

Address: Sharp Hall Rm. 206, 23 The Green

Newark, DE 19717

Telephone: 263-475-6114 Fax: _____

E-mail: ehreed@udel.edu

Permission is granted to reproduce the above-referenced material. Please acknowledge the author(s) and publication data of the original material, and include the words: "Reproduced by permission of The Electrochemical Society."

4/8/14
Date


John Lewis, Associate Director of Publications

Figure A.5: Copyright permission for Figure 3.12, PEO:LiCF₃SO₃ phase diagram.